

University of South Dakota

USD RED

Honors Thesis

Theses, Dissertations, and Student Projects


Spring 4-13-2021

Nitro Group Reduction for Use in Organic, Cathodic Materials

Brock G. Goeden

University of South Dakota

Follow this and additional works at: <https://red.library.usd.edu/honors-thesis>

 Part of the [Analytical Chemistry Commons](#), [Organic Chemistry Commons](#), [Physical Chemistry Commons](#), [Polymer Chemistry Commons](#), and the [Power and Energy Commons](#)

Recommended Citation

Goeden, Brock G., "Nitro Group Reduction for Use in Organic, Cathodic Materials" (2021). *Honors Thesis*. 146.

<https://red.library.usd.edu/honors-thesis/146>

This Honors Thesis is brought to you for free and open access by the Theses, Dissertations, and Student Projects at USD RED. It has been accepted for inclusion in Honors Thesis by an authorized administrator of USD RED. For more information, please contact dloftus@usd.edu.


NITRO GROUP REDUCTION FOR USE IN ORGANIC, CATHODIC MATERIALS

By
Brock Goeden

A Thesis Submitted in Partial Fulfillment of the Requirements for the University of South
Dakota's Honors Program

Department of Chemistry
The University of South Dakota
April 2021

The members of the Committee appointed to examine
the thesis/dissertation of Brock Goeden find it
satisfactory and recommend that it be accepted.

DocuSigned by:

6AE9C17B6D9C488...

Dr. Haoran Sun
Associate Professor of Chemistry (USD)
Director of Committee

DocuSigned by:

E9CCA206A6BE459...

Dr. Pere Miró
Assistant Professor of Chemistry (USD)
Committee Member

DocuSigned by:

F1333D14D2DF41B...

Dr. Miles Koppang
Professor Emeritus of Chemistry (USD)
Committee Member

ABSTRACT

The industrial demand for higher capacity, light-weight battery materials has skyrocketed in recent years due to heavy investments in portable electronics, electronic vehicles, and renewable energy sources. However, rechargeable battery technology has seen little improvement since the invention of the Lithium-Ion battery in the 1980s. The low energy density of the traditionally utilized LiCoO_2 cathodic material (specific capacity: 272 mAh g^{-1}), has limited its potential to meet these increasing demands. To solve this problem, our research group is investigating new types of lightweight, organic, polymeric materials with conductive backbones as a possible replacement for the cathodic materials in Lithium-Ion batteries. These polymers could be utilized as a rechargeable battery material by relying upon the redox couple between the nitroso and phenylhydroxylamine functional groups. These rechargeable materials would have a calculated theoretical capacity of $459.60 \text{ mAh g}^{-1}$ or $433.52 \text{ mAh g}^{-1}$. NMR results show that we have successfully prepared two monomers with thiophene functional groups and another model compound. Initial electrochemical study indicates multiple electron transfer reaction occurs during the reduction at about 2.5 V vs. Li/Li^+ redox couple. Future work would focus on the optimization of polymerization condition of the monomers and to begin preliminary lithium battery discharge testing. This project explores the field of light-weight organic cathodic materials and has the potential to greatly increase the energy density for Lithium-Ion batteries. This would ultimately serve to remove the technology bottleneck that is holding research in other areas back and would be to the benefit of anyone who relies upon battery technology in their daily life.



____ Dr. Haoran Sun (Director)

TABLE OF CONTENTS

Chapter 1. Introduction and Background.....	1
1.1 Battery Background.....	1
1.2 Conversion-Style Organic Cathodes.....	3
1.3 Polymeric Materials as Cathodes.....	3
1.4 Redox Active Functional Group.....	4
1.5 Reaction for Monomer.....	8
Chapter 2. Experimental Details.....	10
2.1 Computational Methods.....	10
2.2 Experimental Conditions – Monomers.....	10
2.3 Methods of Characterization.....	12
2.4 Electrochemical Characterization.....	13
Chapter 3. Experimental Results & Discussion.....	15
3.1 Computational Results.....	15
3.2 Results and Observations of Synthetic Work.....	18
3.3 Results of Characterization – Novel Compounds.....	19
3.4 Electrochemical Results.....	22
Chapter 4. Future Work.....	27
Chapter 5. Conclusion.....	28
References.....	29
Supporting Information.....	31

ACKNOWLEDGEMENTS

A great deal of my time in my undergraduate education was spent conducting chemistry research, and the value of that experience cannot be summarized in a single page. For this invaluable life experience, I would like to thank all of my group members in the Sun-Koppang Research Team, the University of South Dakota's Department of Chemistry, the CFFM at USD, and the U. Discover Research Program. Without the contributions from the members of these organizations, this project would have never been possible.

Dr. Sun & Dr. Koppang – 90% or more of my knowledge in the field of chemistry has come from your tutelage. As my educators, advisors, and advocates, you have both had massive impacts in my life. The continuation of my educational career in medical school would have never been possible without the relationship I have with both of you. I would like to thank-you deeply for all that you have done.

Anji – A full page of writing could not completely express the gratitude that I have for the work you have put in to see this project succeed. We had many late afternoons together in the NMR room, sharing both success and failure along the way. Simply put, this project would never have gotten off the ground without the work that you put in. I appreciate it, sincerely, from the bottom of my heart.

Siyu & Jordan – Thank-you guys for putting-up with my incessant questions. Your patience was greatly appreciated. I learned a tremendous amount from the both of you, both academically and professionally. You both operated as great leaders within the group and role models for individual and team success. I wish you nothing but success in your future endeavors.

Shankar, Jack, Yao – You have all been great help to me along my journey to completing this project. I appreciate your help with the characterization and electrochemical portions of this survey. I wish you all the best.

Belle – You were a great contribution to the team and have much more to offer in the near future. I wish you the best of luck in your work.

Brady – The future's looking bright. Stay on that grind boiii

CHAPTER 1: Introduction and Background

1.1: Battery Overview

With every passing day, technology continues to rapidly evolve. Massive advancements in the field of medicine, energy, transportation, and portable electronics have provided increased opportunities for advancement, extended our lifespans, expanded global markets, and have brought about a great increase in life satisfaction. However, each one of these areas of technological research and development have been hindered in their development. This hindrance is directly related to a bottleneck effect caused by the slow advancement of battery research and design, of which each of these industries heavily rely upon.¹⁻⁴ Since the commercial development of the lithium-ion rechargeable battery in 1991, very slow progress has been made in this field of research. In fact, since the inception of lithium-ion (Li-ion) batteries, battery performance has increased only six-fold, but the performance of electronics powered by these batteries has increased by 10,000% over the same time frame.⁵ This limitation creates a substantial opportunity for progress in an exciting field of research.

These physical limitations, associated with traditional lithium-ion batteries, can be directly attributed to the materials used in their construction and the mechanism by which they operate. Traditional Li-ion batteries contain, at their most basic, three main components: the positive electrode (cathode), the negative electrode (anode), and the electrolyte in

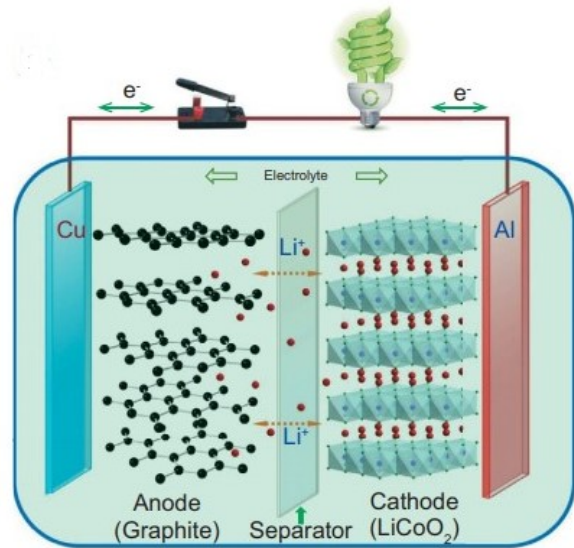


Figure 1: Li-Ion Battery Diagram⁷

between. When the two electrodes are connected via an external circuit, the battery discharges

the energy stored by the cathodic materials spontaneously (electrons through the circuit and lithium-ions in solution). The reverse reaction occurs when a negative, external potential is applied to the battery (anode to cathode) (Figure 1). The flow of lithium-ions only in solution is due to the electrolyte being electronically insulating but ionically conductive and a porous membrane separating the two electrodes.⁶

The most common mechanism by which these reactions occur within commercial Li-ion batteries is intercalation; which is “the process by which a mobile ion or molecule is reversibly incorporated into vacant sites in a crystal lattice”.⁶ There are a variety of reasons as to why initial attempts at Li-ion batteries would capitalize on this mechanism specifically, but it essentially boils down to commercial viability. Regardless of the limited capacities that these styles of batteries offer (Table 1), the seating of alkali ions into their crystal lattice structure results in minimal volume change and mechanical strain on the system. This, in turn, produces a battery that is stable through multiple charge/discharge cycles. The stable product produced through this method may have been functional enough to get mankind this far, but the capacity must improve.

Table 1: Materials Used in Li-Ion Intercalation Style Batteries⁶

	Material	Structure	Average voltage (V vs. Li)	Practical capacity (mAh/g)	Date first reported
Cathodes	LiCoO ₂	Layered	~3.9	~140	1980
	LiMn ₂ O ₄	Spinel	~4.1	~120	1983
	LiFePO ₄	Olivine	~3.45	~160	1997
	LiNi _{1/3} Mn _{1/3} Co _{1/3} O ₂	Layered	~3.8	~200	2001
	LiNi _{0.8} Co _{0.15} Al _{0.05} O ₂	Layered	~3.8	~200	2003
Anodes	Graphite (LiC ₆)	Layered	~0.1	~360	1983
	Li ₄ Ti ₅ O ₁₂	Spinel	~1.5	~175	1994

1.2: Conversion-Style Organic Cathodes

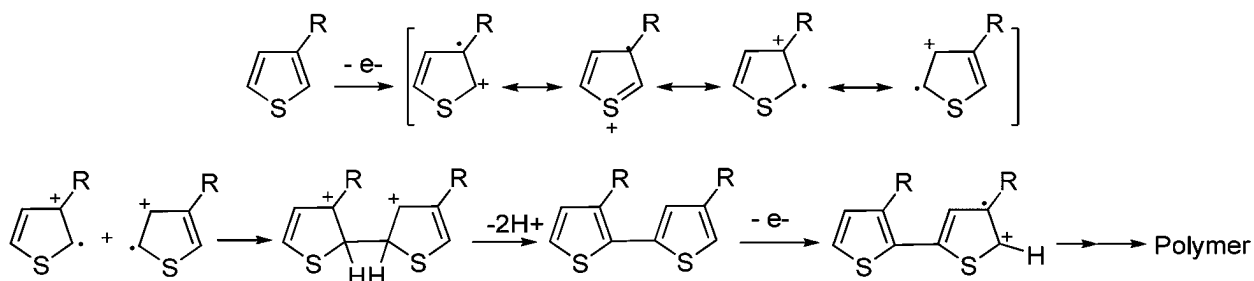
A remedy to this issue can be found through the implementation of chemical reactions within a battery cells that convert the reaction materials to entirely new products through the process of lithiation.⁷ In these batteries, the electric charge is stored via the lithiation (reduction) reaction and discharged upon the reverse reaction (oxidation). These types of batteries are referred to as “conversion-style” batteries. Organic conversion-style batteries, in particular, have the advantage of possessing high theoretical specific capacities, environmental friendliness, modularity, high safety, and natural abundance.⁸ Organic conversion-style batteries have a great deal of promise; however, they can be a double-edged sword. In exchange for greatly increased capacity, the organic conversion-style batteries have limited cycle life. Reducing the cycle life of the materials would slowly degrade the total capacity of the cathodic materials as it undergoes many charge/discharge cycles, yielding a battery not fit to be implemented in a commercial application. The instability of these materials is typically attributable to the propensity of these organic materials to dissolve in the solvents that support the conductive electrolyte.⁹ This issue can be alleviated through the implementation of a polymeric structure in the organic framework of the conversion-style battery. The greatly increased stability of the polymer, compared to individual molecules, would serve to eliminate some of these potential pit-falls; with a fantastic example of this being observed in polymers containing the electrochemically active quinone functional groups.¹⁰

1.3: Polymeric Materials as Cathodes

The options that have been investigated as possibilities for conjugated, aromatic, heterocyclic polymers that are electrochemically polymerizable include: polypyrrole, polythiophene, and polyaniline.¹¹ These polymers are highly promising options for the conductive backbone of an organic, cathodic material due to the incredibly high conductivity of

these organic polymers. The conductive properties of these compounds come from the highly π -conjugated structure of the polymer chains. Polythiophene, specifically, stands out as a potential candidate for constructing an organic, cathodic polymer due to the extremely high conductivity observed in lab ($2\text{-}150\text{ S cm}^{-1}$)¹², the abundance of starting materials, and the ability to form consistent polymer morphologies upon electrodeposition.¹³ The electrodeposition of polythiophene on the surface of an electrode is a highly efficient method for the synthesis of a conductive and pure polymer.¹³ The mechanism for this specific reaction is a radical cationic polymerization¹⁴ (Figure 2).¹⁵ This process would eliminate the need for any adhesives or conductive compounds, such as carbon black, in order to function on the surface of an electrode, as current can be conducted directly through the material once deposited.¹³ This would ultimately increase the capacity of the battery because of the reduction in weight compared to non-electrodeposited compounds.

Figure 2: Mechanism of Radical Polymerization of Thiophene¹⁵

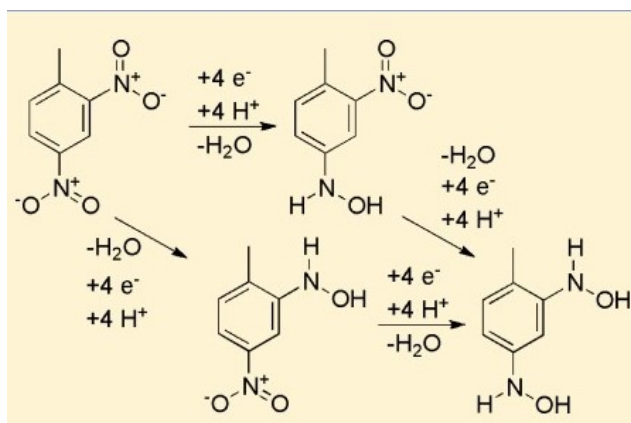


1.4: Redox Active Functional Group

With an ideal candidate for a polymeric backbone established, an electrochemically active portion of the organic cathode must also be established. The ultimate criteria for selection would involve maximizing the theoretical capacity of the cathode. This would involve selecting a reduction mechanism that would store the greatest number of electrons at the lowest possible

weight. For this reason, the nitro group was selected. The reduction of nitro groups is typically associated with the $6 e^-/6 H^+$ reduction to an amine commonly observed in synthetic reactions. However, electrochemical reduction of nitro groups has displayed a different path for reduction. It has been observed in aqueous environments that nitro groups actually undergo a $4 e^-/4 H^+$ reduction to a hydroxylamine group (Figure 3).¹⁶ This corresponds to an impressive theoretical capacity per nitro group. This reduction, however, is not a reversible process. During the reduction process to the phenylhydroxylamine, a water group dissociates from the nitro group.¹⁶ The irreversibility of the process makes it a poor candidate for a rechargeable cathodic material (while still leaving the door open for implementation in a single-use battery).

Figure 3: Reduction of Aromatic Nitro Groups to Phenylhydroxylamine¹⁶



The hydroxylamine group, however, still contains potential as a functional element in a rechargeable battery system. This is because of the electrochemical relationship between the hydroxylamine group and the nitroso group. Electrochemical investigation has shown, that upon reduction from a nitro group to the hydroxylamine group, reversible oxidation is possible to a nitroso group when a more positive potential is applied.¹⁷ This process is a completely reversible $2e^-/2H^+$ redox couple¹⁸ (Figure 4)¹⁹. It can be observed that the two mechanisms of reaction are

interrelated by observing cyclic voltammetry of the reduction, subsequent oxidation, and final reduction of nitrobenzene and the oxidation of phenylhydroxylamine with its subsequent reduction (Figure 5)¹⁹. It would be a quick transition from the well-documented electrochemical results in aqueous environments, to an aprotic, lithium-ion rich solution. This would result in the protons typically used in these redox reactions being replaced by lithium-ions. The results of which are well-documented in the lithiation of organic quinones in aprotic environments.²⁰

Figure 4: Reduction of Nitro Groups¹⁹

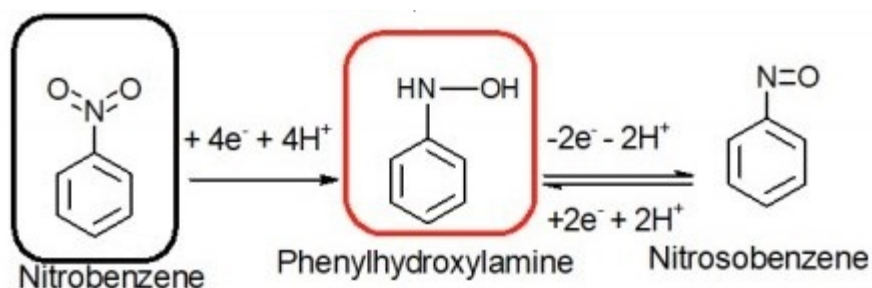
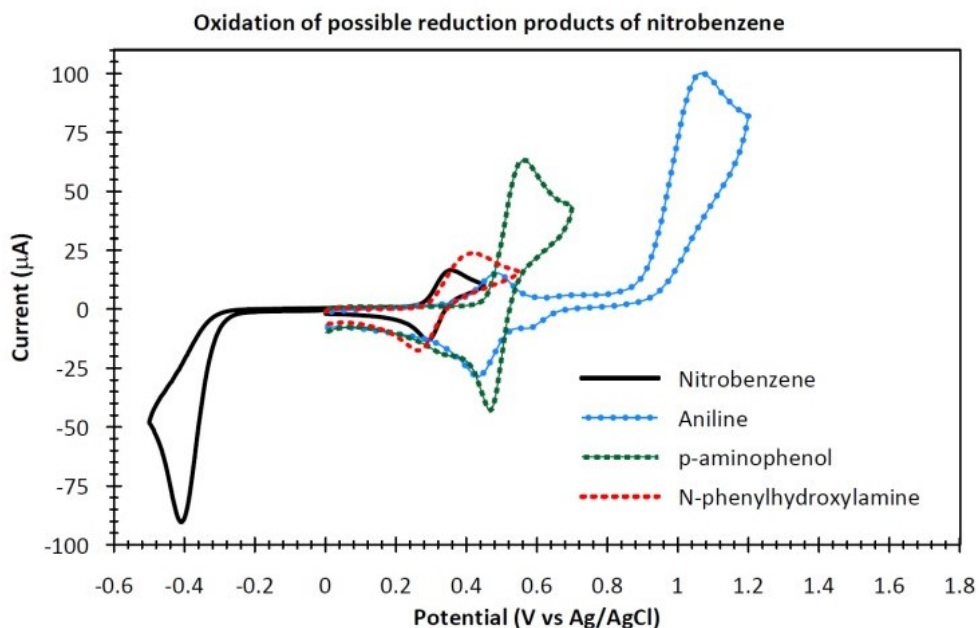


Figure 5: CVs Displaying Electrochemical Activity of Possible Reduction Products of Nitrobenzene¹⁹



1.5: Synthetic Reaction for Monomer Production

The mechanism by which the electrochemically polymerizable thiophene units were introduced to the electrochemically active functional units of the monomer structure is nucleophilic aromatic substitution. Utilizing 2,4-Dinitrofluorobenzene (Sanger's Reagent/DNFB) and aromatic amines as reactants, the nucleophilic replacement of fluoride by the amino group proceeds through a Meisenheimer complex transition state²¹ (Figure 6). The reaction of Sanger's reagent with amino groups was first utilized as early as the 1950s to sequence amino acids²²⁻²³ and eventually became Nobel Prize winning work. Today, the nucleophilic aromatic substitution of Sanger's Reagent provides a quick, simple, and affordable one-step method to create an electrochemically active monomer for use in an organic cathode. By incorporating 2 nitro groups on a single benzene ring, a reversible redox reaction totaling $4e^-/4H^+$ is possible. The three candidates for cathodic materials utilizing a combination the previously mentioned research, along with the theoretical capacities for each compound are listed below (Figure 7). Theoretical capacities were calculated based on the molecular weight of the compounds from the following equation: $Q_{theoretical} = \frac{nF}{3.6 * Mw} \text{ mAh g}^{-1}$ [n = electrons per molecule, F = Faraday Constant ($96,485.3329 \text{ sA mol}^{-1}$), Mw = molecular weight].

Figure 6: Mechanism of Reaction: Nucleophilic Aromatic Substitution – Meisenheimer Complex

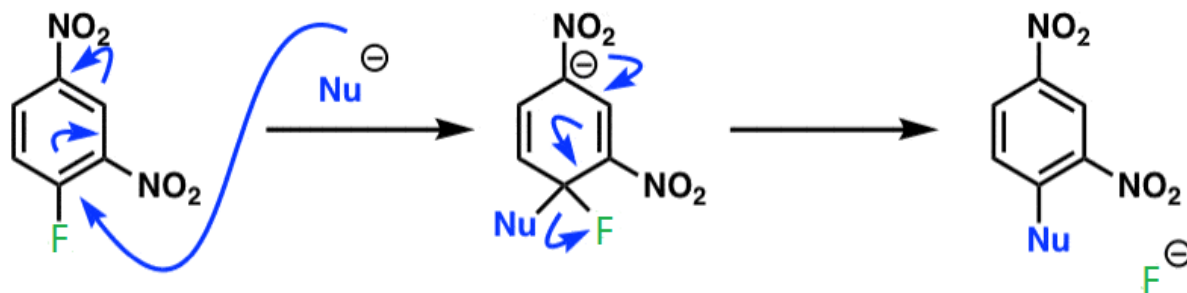
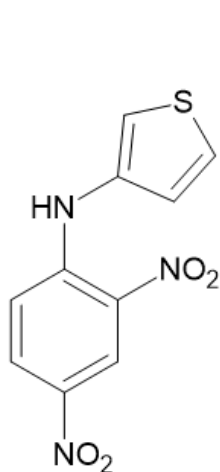
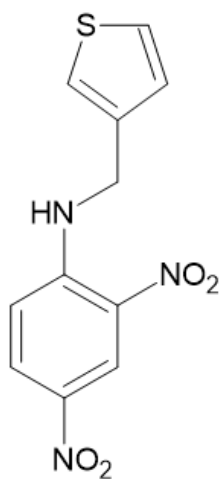


Figure 7: Two Monomer Candidates (left) and Model Compound (right) for Cathodic Materials



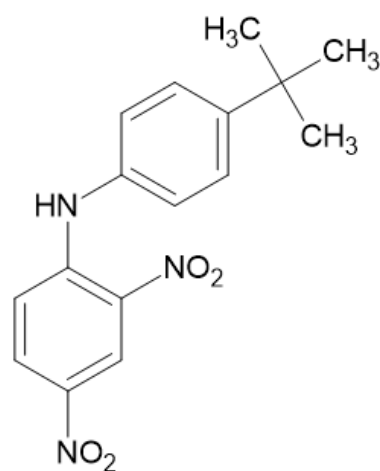
Monomer 1: Mw=265.26
(233.26) g mole⁻¹

**Theoretical Capacity
(Nitroso)** – 459.60 mAh g⁻¹



Monomer 2: Mw=279.29
(247.29) g mole⁻¹

**Theoretical Capacity
(Nitroso)** – 433.52 mAh g⁻¹



Model Compound: Mw=
325.31 (293.31) g mole⁻¹

**Theoretical Capacity
(Nitroso)** – 365.50 mAh g⁻¹

Chapter 2: Experimental Details

2.1: Computational Methods

To examine the viability of the nucleophilic aromatic substitution reaction for the purposes of constructing one of the proposed monomers, computational modelling was employed to help examine the free energy changes of the reactions and electrostatic potential maps of the final products. Structures of the starting materials (2,4-dinitrofluoro benzene and the corresponding aromatic amines) and final products were built in the modelling software Gabedit.²³ Gabedit is a freeware graphical user interface, offering preprocessing and postprocessing tools for editing, displaying, analyzing, converting, and animating molecular systems.²⁴ The command files containing the cartesian coordinates for the atoms in the molecular structures underwent geometric optimization and frequency calculations via the DFT:B3LYP/6-311G(d,p) method. The geometries were set to a tight optimization to ensure adequate convergence and reliable frequencies, with all experiments running the scrf specification in EtOH (mimicking experimental conditions). The command files for these calculations were submitted to the Lawrence Supercomputer at the University of South Dakota. Lawrence operates using the Gaussian09 and Gaussian16 version of the Gaussian computational software package. Results of the computational studies are displayed in section 3.1.

2.2: Experimental Conditions for Nucleophilic Aromatic Substitution

Monomer 1: The nucleophilic aromatic substitution reaction between 3-aminothiophene and 2,4-dinitrofluorobenzene is a 1:1 reaction. A reaction based on a 1-gram scale of the 2,4-dinitrofluorobenzene (Mw=186.1 g/mol) involves 730 mg of 3-aminothiophene hydrochloride (Mw=135.62 g/mol) and 600 mg of potassium carbonate (Mw=138.205 g/mol) to neutralize the

acidic thiophene salt, freeing the amine group for reaction. A total 54 mL of EtOH was utilized as the solvent to ensure 0.1 M concentration, making this reaction essentially a derivative of the reaction conditions used in Sanger's Nobel-Prize winning work.²³ The 2,4-dinitrofluorobenzene and potassium carbonate are initially dissolved in 40 mL of EtOH, and the 3-aminothiophene hydrochloride is dissolved in a separate vial, containing 14 mL of EtOH. The thiophene solution is added dropwise over the course of 45 minutes to prevent oxidation of the freebase 3-aminothiophene that is produced upon introduction to the potassium carbonate. This solution is then allowed to sit for 3 hours in a 100 mL round bottom flask to ensure a complete reaction. The scarlet red precipitate begins to form during the introduction of the reactants and accumulates over the next 3 hours. This product can be purified by simple rinsing with cold methanol. More observations from this experiment can be found in section 3.2, and chemical characterization results can be found in section 3.3.

Monomer 2: The reaction to produce the 2nd monomer is also a 1:1 reaction. Thus, a reaction based on a scale of 500 mg of 2,4-dinitrofluorobenzene involves 0.27 mL of thiophen-3-ylmethanamine (Mw=113.18g and density=1.130 g/mL). No carbonate is required as was the case with the previous reaction, as the amine already exists as a freebase. This reaction was performed at a much greater concentration. 15 mL of EtOH was used resulting in a 0.24 M concentration. The reactants were added simultaneously to the flask. This reaction was allowed to sit for 3 hours but immediately yielded a yellow precipitate. Purification of this product involved recrystallization using dichloroethane as a solvent. Observations from this experiment can be found in section 3.2, and chemical characterization results can be found in section 3.3.

Model Compound: The model compound, created to demonstrate the viability of the nucleophilic aromatic substitution of aromatic amines and the electrochemical properties of dinitro

compounds, is also a 1:1 reaction. So, a reaction based on a 100 mg scale of the 2,4-dinitrofluorobenzene also involves 80.19 mg of p-tert-butylaniline (149.23 g/mol). 5 mL of EtOH was used as the solvent in a 25 mL round bottom flask, resulting in a concentration of .13 M. This reaction was allowed to sit for 3 hours but immediately yielded an orange precipitate. This reaction was purified through recrystallization using isopropanol as a solvent. Observations from this experiment can be found in section 3.2, and chemical characterization results can be found in 3.3.

2.3: Methods of Chemical Characterization

NMR Spectroscopy: Nuclear Magnetic Resonance (NMR) spectroscopy is the single most powerful characterization method available for organic compounds. In this work both one dimensional NMR experiments, as well as two-dimensional experiments were utilized to ensure accurate characterization. These experiments were conducted using the Bruker Ascend™ 400 Hz NMR spectrometer at the University of South Dakota. NMR spectra were processed and analyzed using Bruker Topspin™ software under the supervision and guidance of the NMR specialist at the University of South Dakota. Two-dimensional NMR experiments are important as these spectra allow the experimenter to observe “multiple quantum transitions” that are undetectable by simple one-dimensional experiments.²⁵ COSY, ¹³C DEPT, HSQC, ¹H, and ¹³C NMR experiments were all utilized in this study. COSY displays the electronic effects that adjacent protons have on each other (2D). ¹³C DEPT provides information about the carbon atoms attached to protons within the structure (1D). HSQC provides information about the electronic effects of carbon atoms and their attached protons (2D). The proton experiments provide information about chemical shift and splitting patterns for the protons in the structure,

and the carbon-13 experiment provides the same information for the carbon atoms in the structure. The results from these experiments can be found in section 3.3 and discussion in 4.1.

X-ray Crystallography: X-ray crystallographic techniques were utilized in this research project to further affirm synthetic results. The single-crystals of the organic products were made via a simple and commonly used evaporation technique.²⁶ Upon successful crystal growth, the crystal structure was determined using the Bruker D8 VentureTM x-ray diffractometer. The data collection software for this process was the Bruker Apex3TM software, and the crystal structures were solved in the WinGXTM software and SHELXTM software. For the solved crystal structures, refer to section 3.3, and for the discussion over the data, refer to section 4.1.

High-Resolution Mass Spectrometry: High-resolution mass spectrometry (HRMS) is a very powerful characterization tool for synthetic chemists. HRMS features both high resolution mass accuracy and allows for the analysis and quantitation of compounds, determination of elemental compositions, and identification of unknowns.²⁷ HRMS is used to confirm the presence of a compound synthesized via the molecular mass of the compound.

2.4: Electrochemical Characterization

The field of electrochemistry relates the flow of electrons to chemical changes. The primary method utilized in this study for the electrochemical characterization of compounds is cyclic voltammetry (CV). This method is a very powerful tool for probing reactions involving electron transfers, and provides a plethora of information regarding the electronic properties of a wide-range of materials.²⁸ CVs are recorded as voltammograms, with the x-axis (typically) representing the voltage (V) applied to a system and the y-axis representing the current (i) passed through a solution (Figure 7).²⁸ The curves in the current vs potential line graphs correspond the

diffusion-controlled reduction and oxidation of a species in solution (the reduced/oxidized species takes time to diffuse away so the current does not simply hit the max current depending on the solution concentration and, rather, follows a curved shape).²⁸

Electrochemical cells used in this study's experiments were constructed in glass vials using a three-electrode set-up. The working electrode, which shifts potential along with the voltammogram and provides the surface for the electrochemical reactions to occur upon, is a 3 mm diameter glassy carbon electrode. Glassy carbon is used because of its chemical stability and ability to be easily resurfaced, which is important for ensuring facile and reproducible electron transfer in solution.²⁹ The potential of the working electrode is controlled in comparison to the reference electrode which is also in solution. Typically, a reference electrode is isolated from the system and contains a solution with a known concentration of ions where the potential difference between the two systems can be determined. In a lithium-rich environment, however, a true reference electrode cannot be used because of the water that would be introduced to the system. So, a quasi-reference electrode made of a silver/silver chloride wire was used. While not a perfect substitute, the wire will maintain a quasi "constant" potential during the experiments. Finally, the counter electrode in these experiments is a 99.95% pure platinum wire, coiled to increase surface area. The counter electrode has the opposite potential as the working electrode, and the opposite reaction occurs at the counter electrode to ensure that charge balance is maintained within the solution.²⁸ All experiments were conducted in MBraun Labstar 1200 Argon glovebox (to prevent air/water-lithium reactions) using an Autolab PGSTAT302N potentiostat under the command of the Nova 2.0 software. Results of these experiments can be found in section 3.4, and the discussion on this topic can be found in section 4.3.

Chapter 3: Results and Discussion

3.1: Results of Computational Studies

Monomer 1: Results

Change in free energy (ΔG_{total}) = (Sum of Free Energy of Products) – (Sum of Free energy of Reactants)

Free Energy Change: [HF (-63,052.668 kcal/mole) + Monomer 1 (-783,455.4132 kcal/mole)] – [3-aminothiophene (-381765.4943 kcal/mole) + DNFB (-464738.5687 kcal/mole)] = ΔG_{total} = -4.018 kcal/mole

Figure 8: 3-aminothiophene Optimized Structure

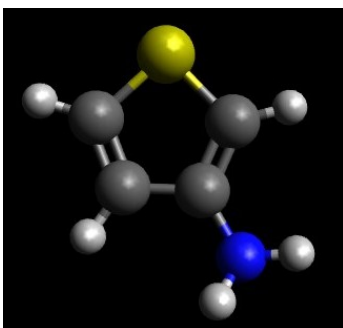


Figure 9: DNFB Optimized

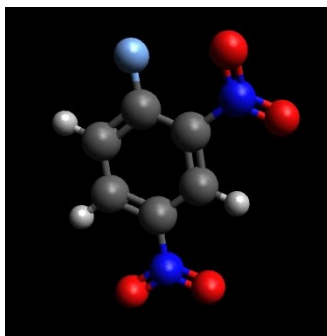


Figure 10: DNFB ESP Map

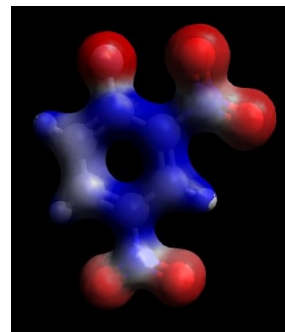


Figure 11: Monomer 1 – Optimized Structure

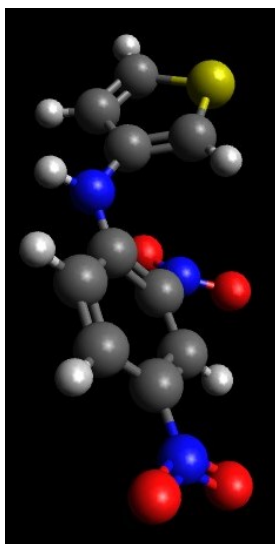


Figure 12: Monomer 1 – ES Map

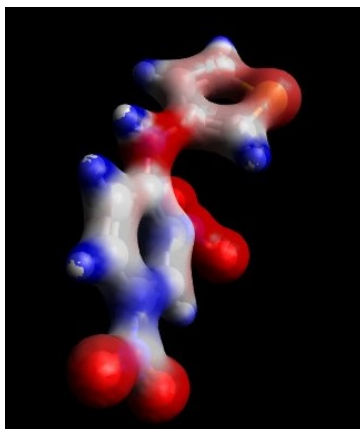


Figure 13: Monomer 1 – HOMO

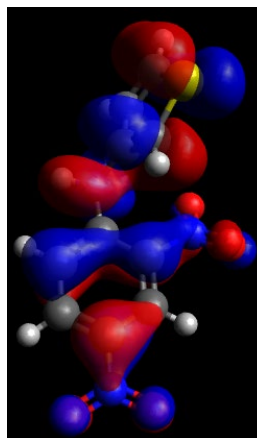
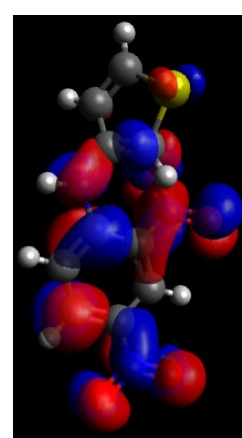


Figure 14: Monomer 1 – LUMO



Monomer 2: Results

Free Energy Change: [HF (-63,052.668 kcal/mole) + Monomer 2 (-808,106.0171 kcal/mole)] – [thiophen-3-ylmethanamine (-406,417.3514 kcal/mole) + DNFB (-464738.5687 kcal/mole)] = $\Delta G_{\text{total}} = -2.765$ kcal/mole

Figure 15: Thiophen-3-ylmethanamine Optimized

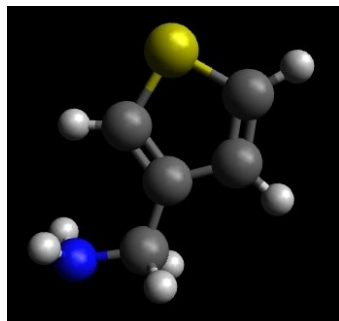


Figure 16: DNFB Optimized

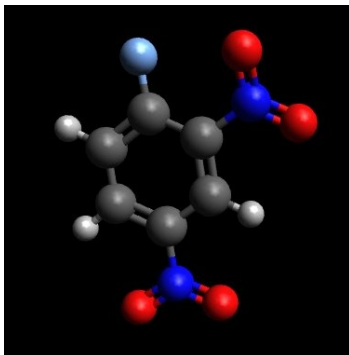


Figure 17: DNFB ESP Map

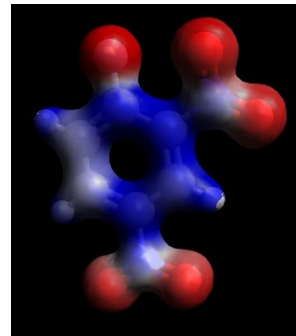


Figure 18: Monomer 2 – Optimized Structure

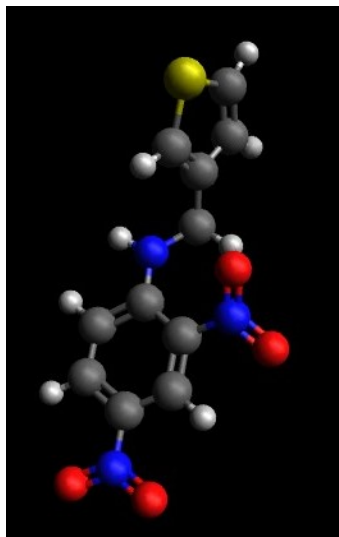


Figure 19: Monomer 2 – ESP Map



Figure 20: Monomer 2 – HOMO

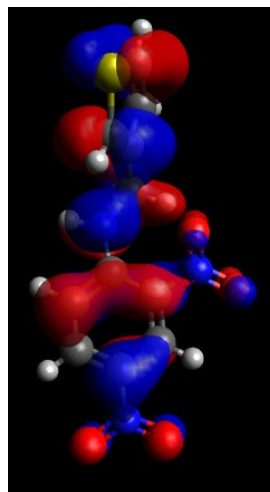
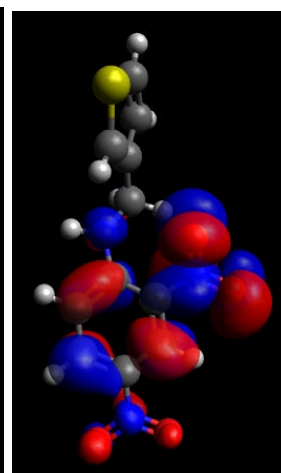


Figure 21: Monomer 2 – LUMO



Model Compound: Results

Free Energy Change: [HF (-63,052.668 kcal/mole) + Model Comp (-680,793.8028 kcal/mole)] – [p-tert-butylaniline (-279106.3167 kcal/mole) + DNFB (-464738.5687 kcal/mole)]
= $\Delta G_{\text{total}} = -1.585$ kcal/mole

Figure 22: P-tert-butylaniline Optimized

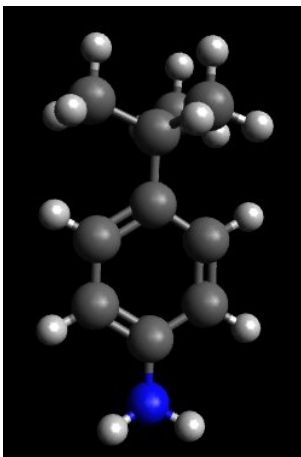


Figure 23: DNFB Optimized Structure

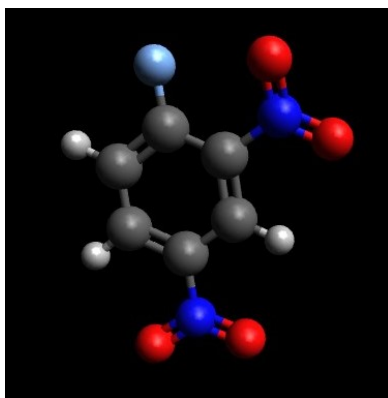


Figure 24: DNFB – ESP Map

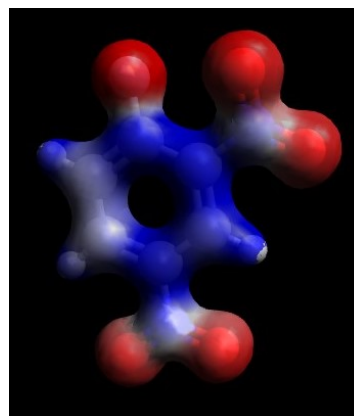


Figure 25: Model Compound Optimized Structure

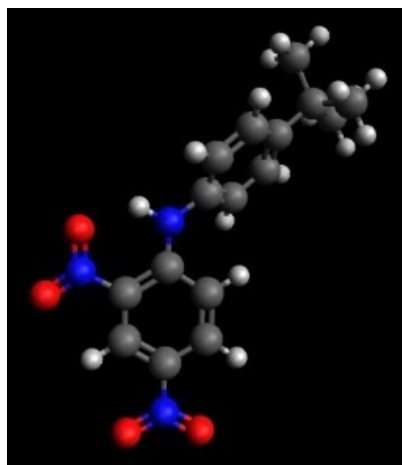


Figure 26: Model Compound ESP Map

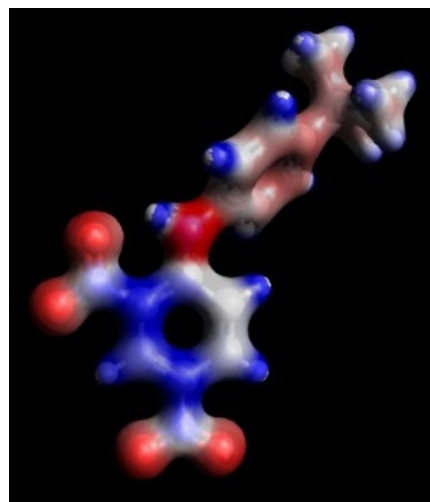


Figure 27: Model
Compound HOMO

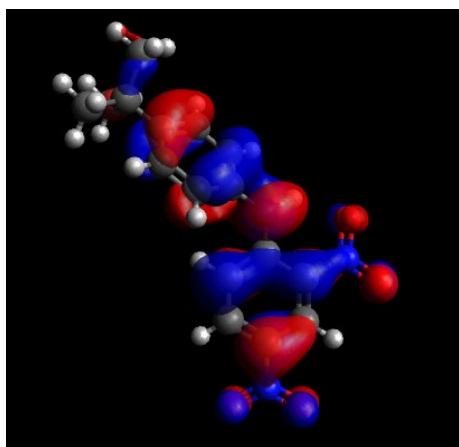
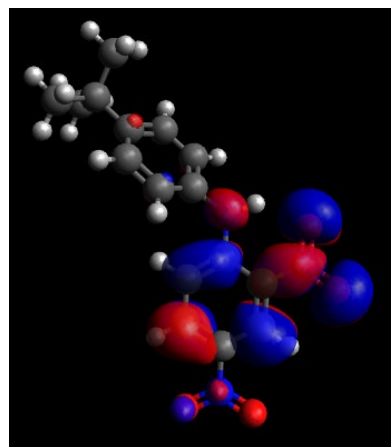


Figure 28: Model
Compound LUMO



Discussion:

Computational modeling has shown that the free energy change of all three reactions is negative. These calculations indicate that all three reactions should, in theory, be spontaneous. Monomer 1 had a total free energy change of -4.018 kcal/mole, Monomer 2 had a total free energy change of -2.765 kcal/mole, and the model compound had a total free energy change of -1.585 kcal/mole. These results provide enough information to proceed with the reactions in a laboratory setting. The optimized structure of the model compound aligns to a near identical match with the crystal structure displayed in section 3.3 (N-H and O-N should, in theory, interact in all compounds). Aside from these free energy calculations, the frequency calculations for these compounds yielded a great deal of information when mapping the electrostatic potentials and HOMOs and LUMOs. From the ESP maps, it can be observed that the greatest electron donating effects from the electron rich aromatic ring to the electron deficient ring is displayed by Monomer 1. This is worth noting because it indicates that the electrons may be more delocalized through the entire molecule in Monomer 1 more so than Monomer 2. The HOMO-LUMO

surface also provide some interesting information. In these models, the LUMO for these compounds is on the nitrogen of the nitro groups. So, theoretically, the first electron added to these systems through an electrochemical reduction would be placed within that orbital, and this finding corroborates the understood mechanism of reduction.³⁰

3.2: Results and Observations of Synthetic Work

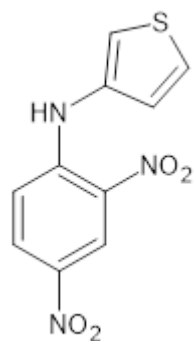
For Monomer 1, the reaction yields a scarlet red powder when given enough time for the nucleophilic substitution reaction to proceed. At the concentration given in the experimental details section (.1 M), this is typically around an hour before a satisfactory yield is achieved. However, this reaction becomes almost instantaneous when the concentration is increased. After purification, either by simple rinsing or recrystallization, the scarlet red substance takes the form of thin, red fibers. After drying, the bulk substance is light and airy, and it displays electrostatic properties. When dissolved, its solution is yellow which is worth noting.

For Monomer 2, the reaction yields a neon yellow powder. This reaction was conducted at a higher concentration and yielded a precipitate instantaneously with good yield. This product was unable to be purified by simple rinsing with an alcohol. TLC results showed the presence of two compounds with similar chemical properties in differing amounts. Pure product could be obtained through recrystallization. The solvent used in the recrystallization of this compound is dichloroethane, due to the high boiling point (70.5 °C) and the compounds excellent solubility in it. Purified product takes the form of thin, yellow, needle-like crystals.

For the model compound, the reaction yields a neon orange powder. This reaction was also conducted at a higher concentration and yielded a precipitate instantaneously with good yield. This product was able to be purified through simple rinsing with alcohol (MeOH). This

compound, when purified, took on the form of thin, orange, needle-like crystals. This compound also generates a yellow solution when dissolved like Monomer 1.

3.3: Results of Characterization – Novel Compounds



¹H NMR (400 MHz, DMSO-*d*₆) δ 10.07 (s, 1H), 8.901-8.984 (d, 1H), 8.293-8.262 (dd, 1H), 7.731-7.710 (dd, 1H), 7.582-7.570 (dd, 1H), 7.196-7.190 (m, 1H), 7.181-7.172 (m, 1H); **¹³C DEPT NMR** (1400 MHz, DMSO-*d*₆) 130.5, 127.6, 125.96, 123.83, 119.62, 117.44. (Pictures in Supporting Information – Above, COSY, HSQC)

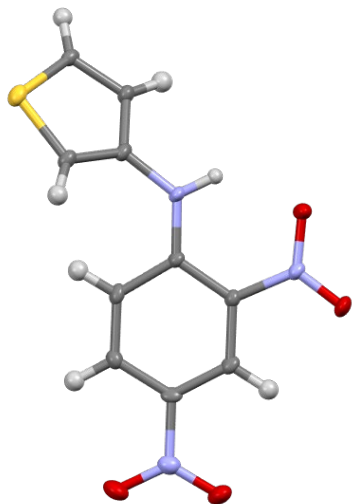


Figure 29: Crystal Structure of Monomer 1

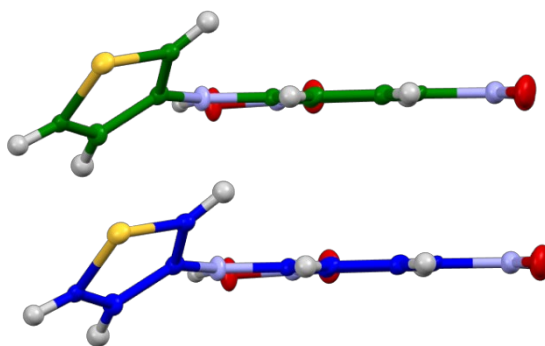
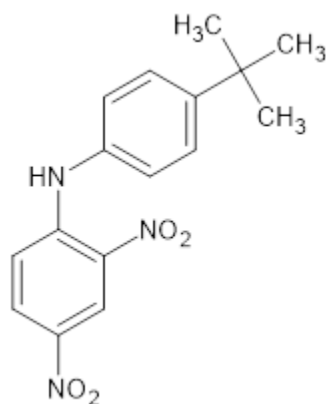


Figure 30: Dimer View of Monomer 1



¹H NMR (400 MHz, DMSO-d₆) δ 10.116 (s, 1H), 8.898-8.891 (d, 1H), 8.24-8.21 (dd, 1H), 7.542- 7.521 (dd, 2H), 7.327-7.306 (dd, 2H), 7.106-7.082 (d, 1H), 1.321 (s, ~8H (*should be 9)); **¹³C DEPT NMR** (1400 MHz, DMSO-d₆) δ 130, 127.04, 125.96, 124, 117.3. (Pictures in Supporting Information – Above, COSY, HSQC)

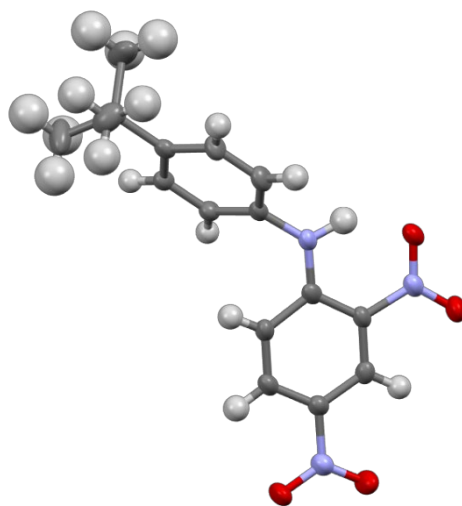


Figure 26: Crystal Structure of Model Compound

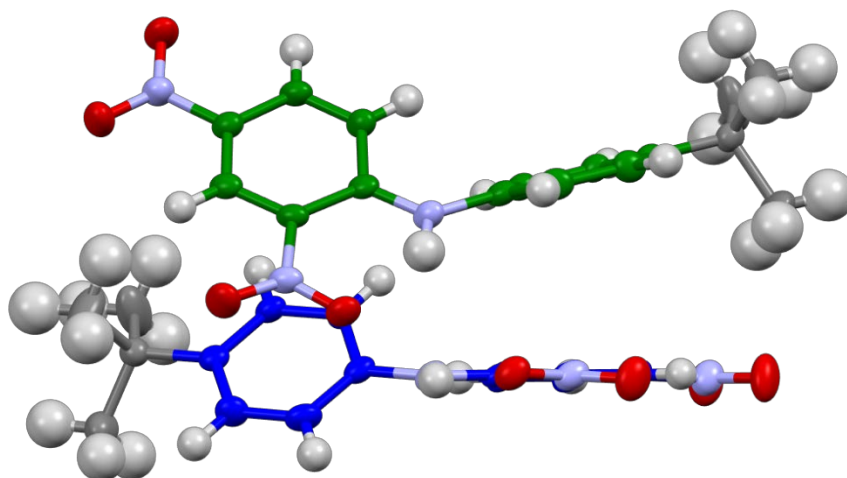
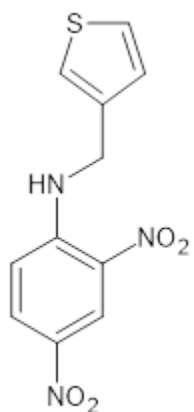


Figure 27: Dimer View of Model Compound



¹H NMR (400 MHz, CDCl₃) δ 9.176-9.169 (d, 1H), 8.884 (s, 1H), 8.291-8.261 (dd, 1H), 7.430- 7.410 (dd, 1H), 7.280-7.263 (m?, 1H), 7.106-7.090 (dd, 1H), 9.989-6.965 (d, 1H), 4.69-4.67 (d, 2H); **¹³C DEPT NMR** (1400 MHz, CDCl₃) δ 130.40, δ 127.62, δ 126.36, δ 124.23, δ 122.74, δ 114.25; **¹³C NMR** (1400 MHz, CDCl₃) δ 148.05, δ 136.49, δ 136.36, δ 130.75, δ 130.40, δ 127.62, δ 126.35, δ 124.23, δ 122.74, δ 114.24; **HRMS**: Base peak (M+H) at 280.0382 amu. (Pictures in Supporting Information – Above, COSY, HSQC)

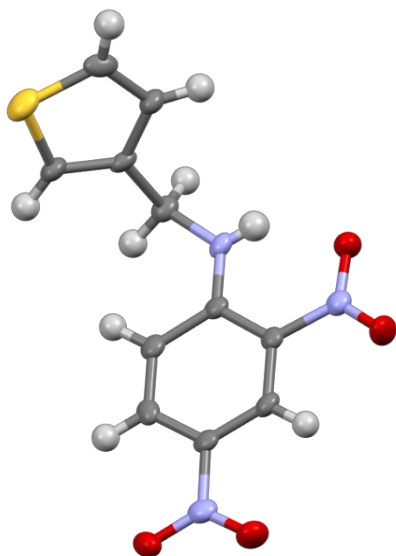


Figure 28: Crystal Structure of Monomer 2

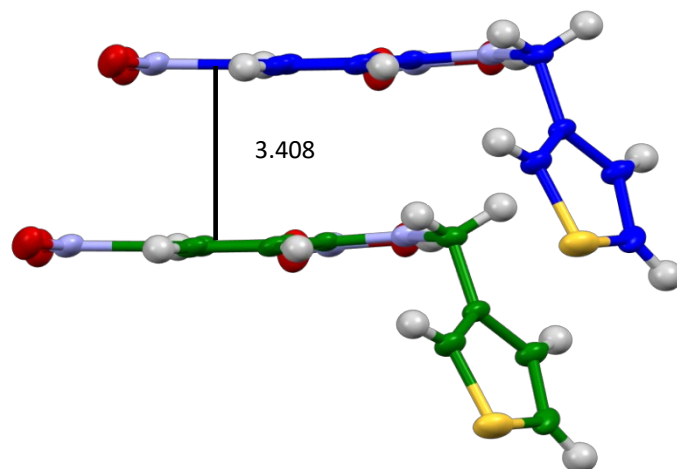


Figure 29: Interplanar Distance between Dimers of Monomer 2

Discussion – Characterization:

The characterization work conducted on each of these compounds confirms the structure of the compounds as predicted by the computational modelling. Analysis of the NMR spectra confirm the position and relationship of the hydrogen atoms and carbon atoms in the structures. The crystal structures for Monomer 2 and the Model Compound further affirm the fact that the nucleophilic aromatic substitution has occurred. HRMS was conducted on Monomer 2 as well, and the base peak corresponding to the M+H ion can be located at 280.0382 amu (which corroborates the calculated Mw of 279.29). The conclusion that can be drawn from the sum of these characterization methods is that a novel application of the Sanger's Reagent has been successfully implemented.

3.4: Electrochemical Results

Monomer 1:

Figure 30: Reduction of Monomer 1 in DFB//TBAPF₆

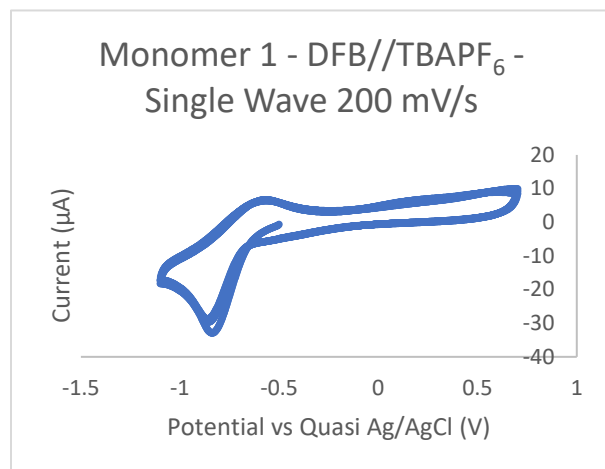
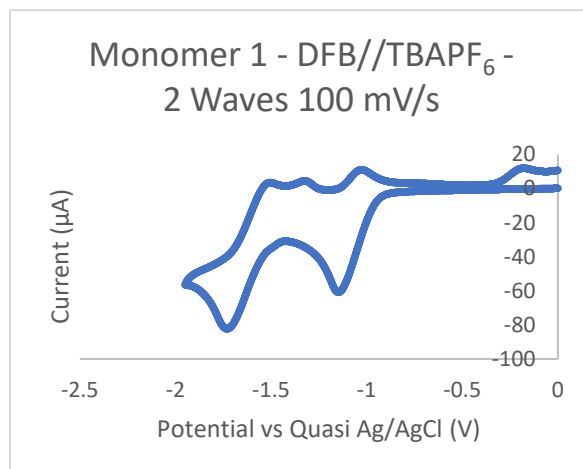


Figure 31: Reduction of Monomer 1 in DFB//TBAPF₆ (2 Waves)



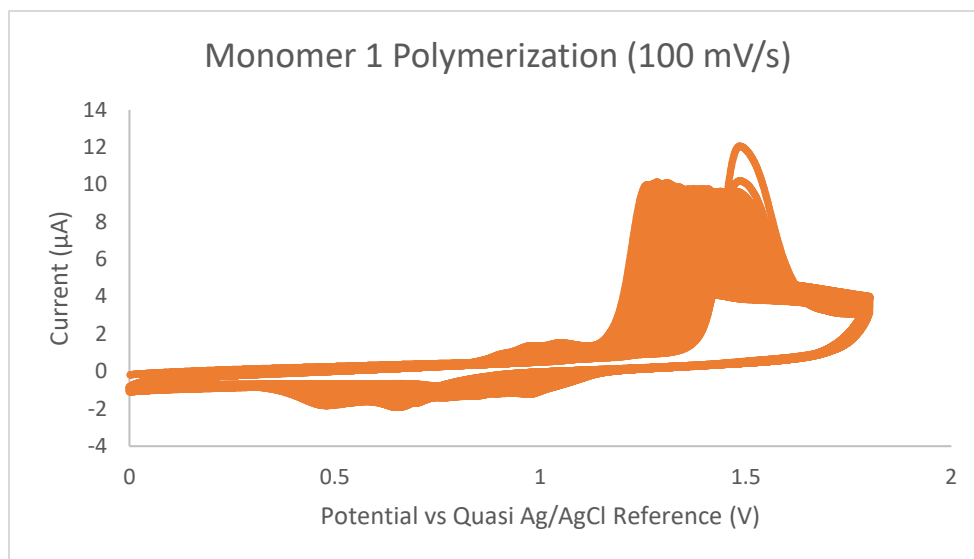


Figure 32: Oxidative Polymerization of Monomer 1

Monomer 2:

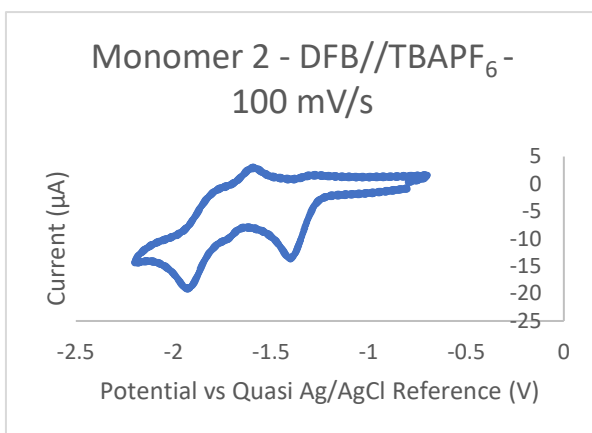


Figure 33: Reduction of Monomer 2 in DFB//TBAPF₆ (2 Waves)

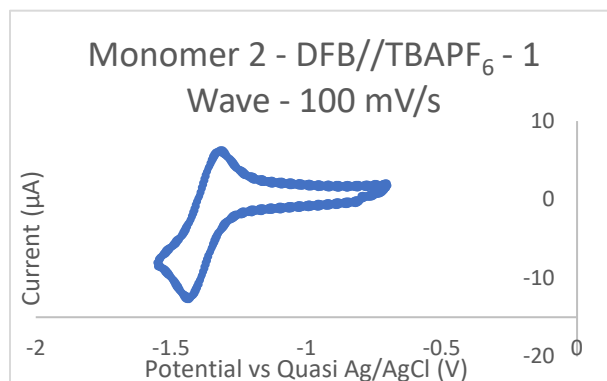


Figure 34: Reduction of Monomer 2 in DFB//TBAPF₆

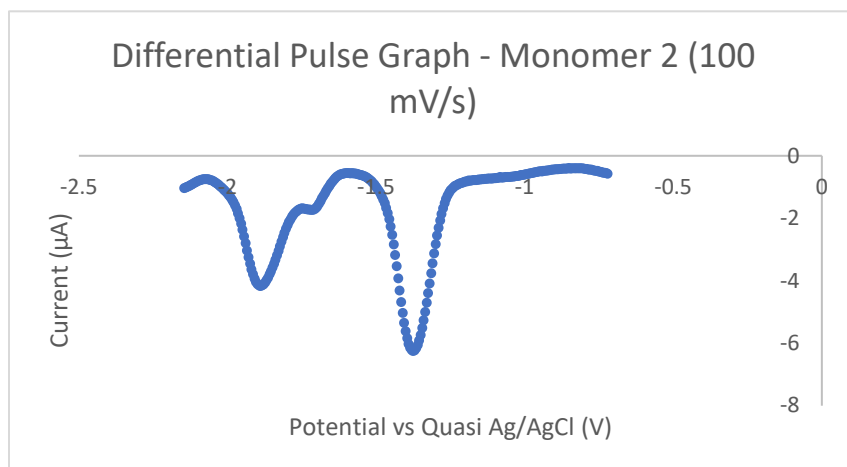


Figure 35: Differential Pulse Scan of Monomer 2

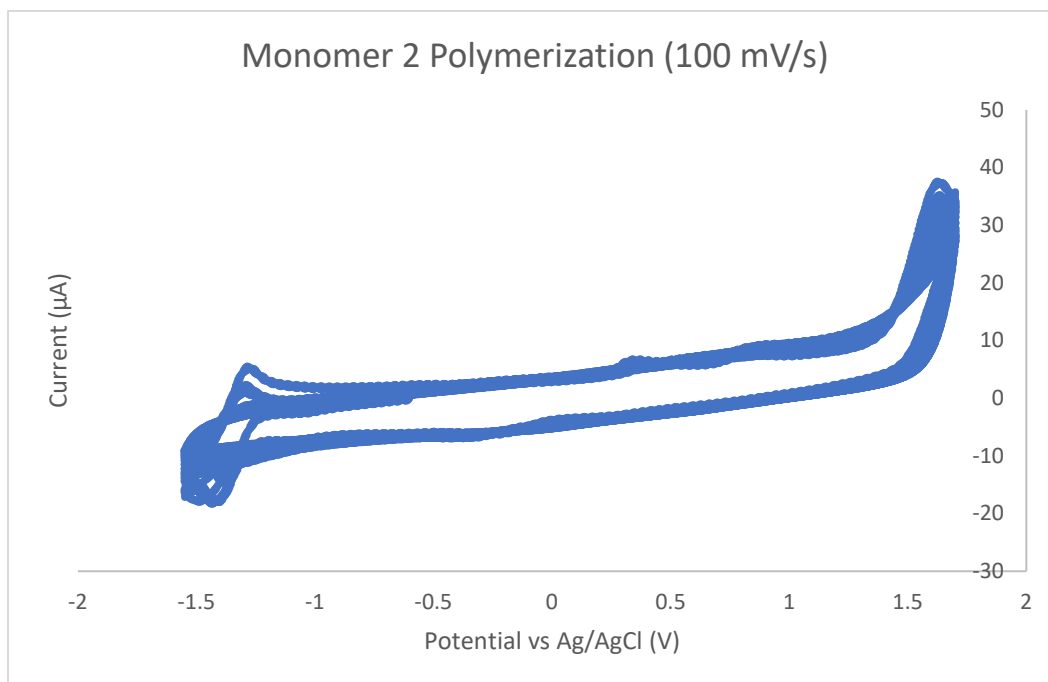


Figure 36: Oxidative Polymerization of Monomer 2 in DFB//TBAPF₆

Model Compound:

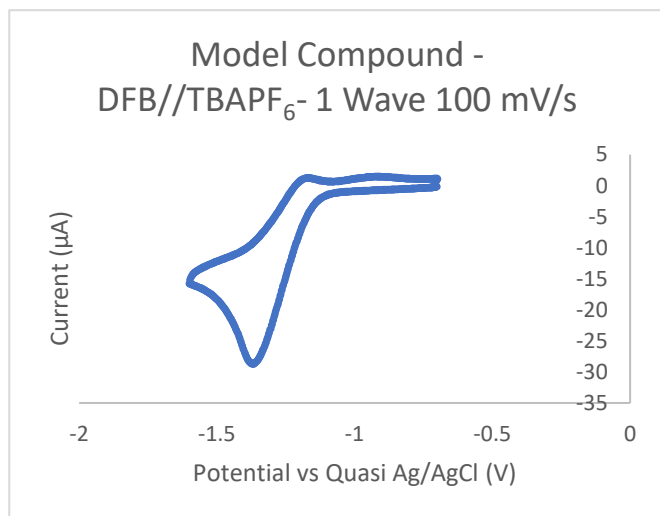


Figure 37: Reduction of Model Compound in DFB//TBAPF₆

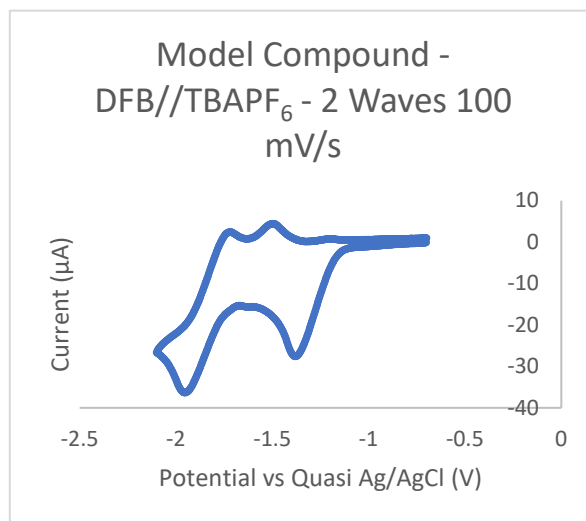


Figure 37: Reduction of Model Compound in DFB//TBAPF₆

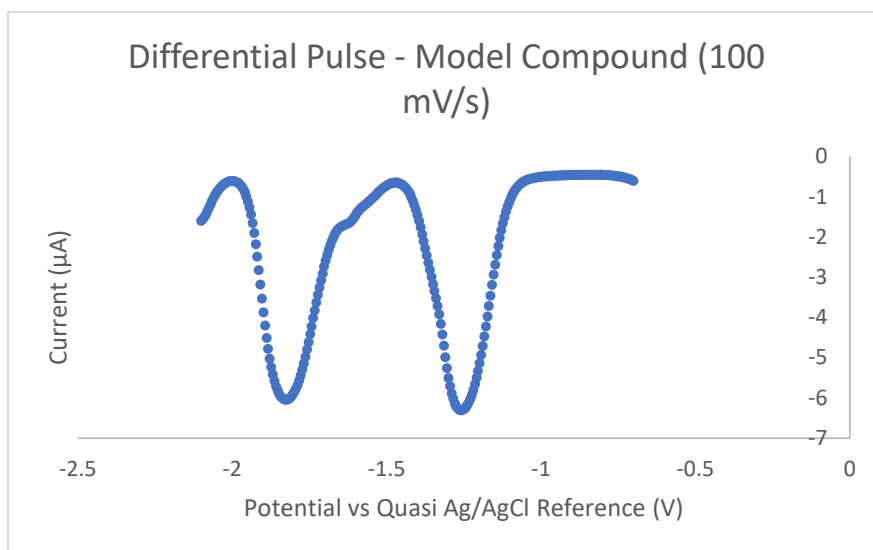


Figure 38: Differential Pulse Scan of Model Compound in DFB//TBAPF₆

Discussion:

Electrochemical reduction of Monomer 1 in an aprotic environment yields two distinct reduction waves, with one smaller wave that appears as a shoulder at -1.5V. The second reduction wave appears to be a reversible process, and the first wave does not. Upon further investigation, the first wave begins to become more easily reversible as the scan rate increases (see supporting information). The oxidation scans of this compound display the polymerization and electrodeposition of the thiophene units on the surface of the electrode. After initial decrease in current, the current slowly begins to climb back up during repetitive scans. The electrochemical reduction of Monomer 2 looks strikingly similar to the reduction of Monomer 1. However, the shoulder is much more pronounced in these scans. The first reduction wave is also a completely reversible process at scan rates of 10 mV/s to 300+ mV/s (see supporting information). The differential pulse scan was utilized to resolve the shoulder from the other two reduction waves. Electrochemical polymerization of the thiophene units is not quite as clean of a process as it was with Monomer 1. The oxidation wave is apparent in the positive region of the

scan, but the current decreases upon subsequent oxidation cycle. The model compound also appears to have similar electrochemical properties to the other two monomers. However, the first reduction wave is much less reversible upon increasing the scan rate (see supporting information). A differential pulse scan was also used on this compound to resolve the shoulder from the other two reduction waves. Overall, the reduction scans indicate that all compounds are electrochemically active, and the oxidation scans indicate that both Monomer 1 and Monomer 2 appear to be polymerizable.

Chapter 4: Future Work

Clearly, this project encompasses a variety of disciplines and has been elucidated from many hours' worth of work. Still, there are many future avenues that can be pursued to further refine some of the results presented in this study. This would encompass further electrochemical characterization of these compounds. Including, refinement of electrodeposition of the thiophene polymer of the surface of an electrode, characterization of the morphology of the polymer, and eventual electrochemical testing of the polymer. It would also include work in alkali, non-aqueous environments with both the monomers in this study and the polymers that can be produced from these compounds. This would paint a much clearer picture of the practical abilities of these compounds as cathodes in real-world battery cells.

Aside from work done on these compounds alone, incorporation of more functional groups within the compounds and further refinement of the chemical structure of these electrochemically active compounds would yield compounds with even higher energy density than the compounds proposed. One compound, that has shown promise for this purpose, is the aromatic imine bond,³¹ and our group has already experimented with some compounds featuring this structure. These novel compounds would undergo a similar computational modeling/chemical and electrochemical characterization process as the compounds in this study. To this point, enough data has been gathered to confirm the identity of the compounds discussed in the study. However, further information such as the final crystal structure for Monomer 1 as well as an HR-MS study of Monomer 1 and the Model compound would serve to cement the findings of the NMR studies.

Chapter 5: Conclusion

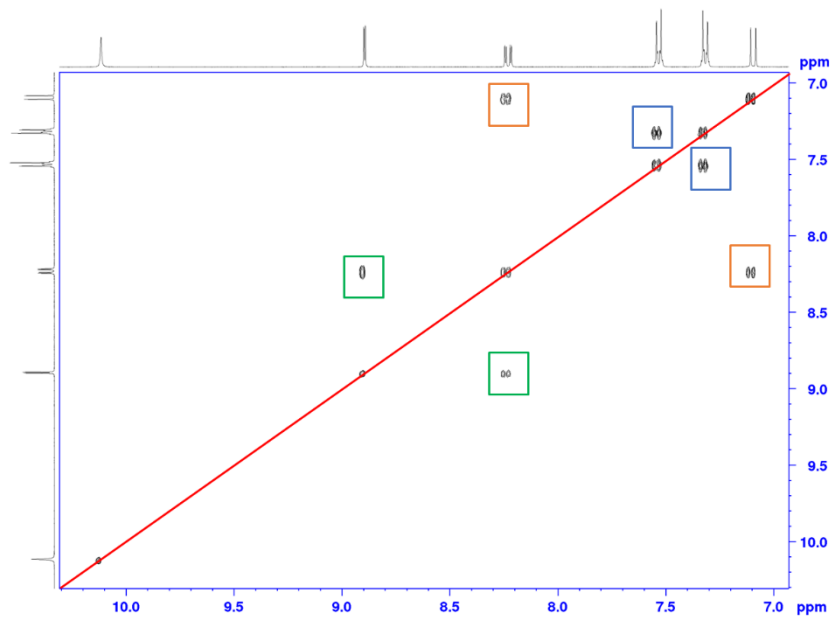
In conclusion, a possible alternative to the traditionally utilized lithium-metal oxide intercalation-style batteries has been proposed. Three compounds, all with theoretical capacities greater than traditional cathodic materials, have been designed, synthesized, and characterized (both chemically and electrochemically). With much work left to be done, the current findings of this study suggest that Sanger's Reagent (2,4-dinitrofluorobenzene) is a practical candidate for the design and synthesis of dinitro compounds for use as organic, cathodic materials. This work has the propensity to drastically change the pace of development in the rechargeable battery industry and could finally widen the bottleneck that is hindering the success of nearly all other tech industries once completed.

References

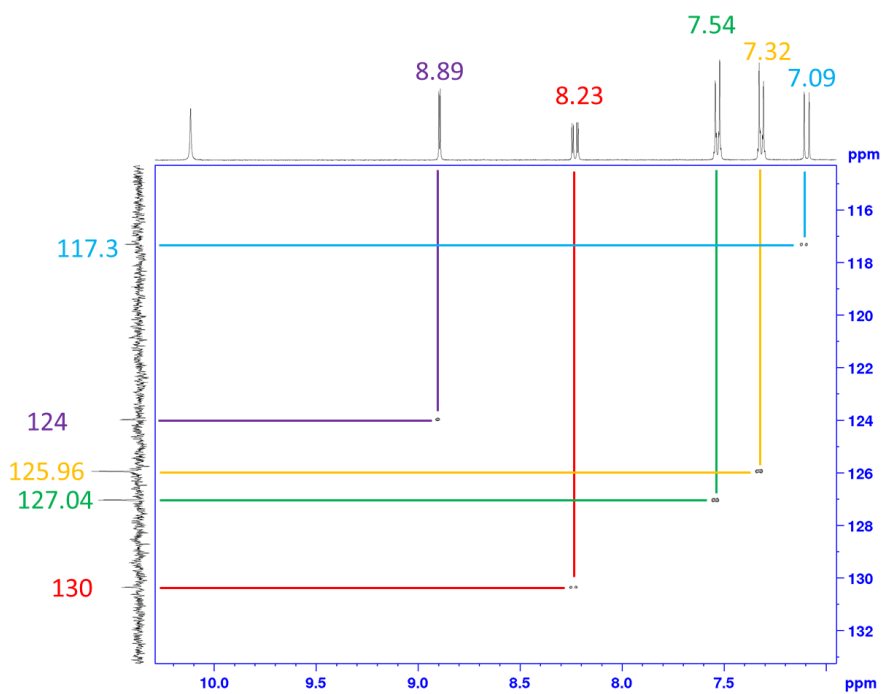
1. Scrosati, B., Power sources for portable electronics and hybrid cars: lithium batteries and fuel cells. *The Chemical Record* **2005**, *5* (5), 286-297.
2. Bock, D. C.; Marschilok, A. C.; Takeuchi, K. J.; Takeuchi, E. S., Batteries used to power implantable biomedical devices. *Electrochimica Acta* **2012**, *84*, 155-164.
3. Tran, M.; Banister, D.; Bishop, J. D. K.; McCulloch, M. D., Realizing the electric-vehicle revolution. *Nature Climate Change* **2012**, *2* (5), 328-333.
4. Dunn, B.; Kamath, H.; Tarascon, J.-M., Electrical Energy Storage for the Grid: A Battery of Choices. *Science* **2011**, *334* (6058), 928.
5. Ross, D., Battery bottleneck [Editorial]. *Engineering & Technology* **2010**, *5* (9), 4-4.
6. Massé, R. C.; Liu, C.; Li, Y.; Mai, L.; Cao, G., Energy storage through intercalation reactions: electrodes for rechargeable batteries. *National Science Review* **2017**, *4* (1), 26-53.
7. Yu, S.-H.; Feng, X.; Zhang, N.; Seok, J.; Abruña, H. D., Understanding Conversion-Type Electrodes for Lithium Rechargeable Batteries. *Accounts of Chemical Research* **2018**, *51* (2), 273-281.
8. Lyu, H.; Sun, X.-G.; Dai, S., Organic Cathode Materials for Lithium-Ion Batteries: Past, Present, and Future. *Advanced Energy and Sustainability Research* **2021**, *2* (1), 2000044.
9. Lu, Y.; Chen, J., Prospects of organic electrode materials for practical lithium batteries. *Nature Reviews Chemistry* **2020**, *4* (3), 127-142.
10. Sieuw, L.; Jouhara, A.; Quarez, É.; Auger, C.; Gohy, J.-F.; Poizot, P.; Vlad, A., A H-bond stabilized quinone electrode material for Li-organic batteries: the strength of weak bonds. *Chemical Science* **2019**, *10* (2), 418-426.
11. Hong, X.; Liu, Y.; Li, Y.; Wang, X.; Fu, J.; Wang, X., Application Progress of Polyaniline, Polypyrrole and Polythiophene in Lithium-Sulfur Batteries. *Polymers* **2020**, *12* (2).
12. Shi, Y.; Peng, L.; Ding, Y.; Zhao, Y.; Yu, G., Nanostructured conductive polymers for advanced energy storage. *Chemical Society Reviews* **2015**, *44* (19), 6684-6696.
13. Xia, C.; Fan, X.; Park, M.-k.; Advincula, R. C., Ultrathin Film Electrodeposition of Polythiophene Conjugated Networks through a Polymer Precursor Route. *Langmuir* **2001**, *17* (25), 7893-7898.
14. Yagci, Y.; Jockusch, S.; Turro, N. J., Mechanism of Photoinduced Step Polymerization of Thiophene by Onium Salts: Reactions of Phenyliodonium and Diphenylsulfonium Radical Cations with Thiophene. *Macromolecules* **2007**, *40* (13), 4481-4485.
15. Khalid, H.; Yu, H.; Wang, L.; Amer, W. A.; Akram, M.; Abbasi, N. M.; ul-Abdin, Z.; Saleem, M., Synthesis of ferrocene-based polythiophenes and their applications. *Polymer Chemistry* **2014**, *5* (24), 6879-6892.
16. Olson, E. J.; Isley, W. C.; Brennan, J. E.; Cramer, C. J.; Bühlmann, P., Electrochemical Reduction of 2,4-Dinitrotoluene in Aprotic and pH-Buffered Media. *The Journal of Physical Chemistry C* **2015**, *119* (23), 13088-13097.
17. Becker Ar Fau - Sternson, L. A.; Sternson, L. A., Oxidation of phenylhydroxylamine in aqueous solution: a model for study of the carcinogenic effect of primary aromatic amines. (0027-8424 (Print)).
18. Li, Y.-P.; Cao, H.-B.; Liu, C.-M.; Zhang, Y., Electrochemical reduction of nitrobenzene at carbon nanotube electrode. *Journal of Hazardous Materials* **2007**, *148* (1), 158-163.
19. Balasingam, M. Electrochemical Reduction of Aromatic Nitro Compounds: Strategies for LC-EC Analysis of Sanger Tagged Analytes. University of South Dakota, Vermillion, SD, 2018.
20. Wang, H.; Emanuelsson, R.; Liu, H.; Edström, K.; Mamedov, F.; Strømme, M.; Sjödin, M., Redox-State-Dependent Interplay between Pendant Group and Conducting Polymer Backbone in Quinone-Based Conducting Redox Polymers for Lithium Ion Batteries. *ACS Applied Energy Materials* **2019**, *2* (10), 7162-7170.

21. Mottishaw, J. D.; Erck, A. R.; Kramer, J. H.; Sun, H.; Koppang, M., Electrostatic Potential Maps and Natural Bond Orbital Analysis: Visualization and Conceptualization of Reactivity in Sanger's Reagent. *Journal of Chemical Education* **2015**, *92* (11), 1846-1852.
22. Harris, J. I.; Roos, P., Amino-acid Sequence of a Melanophore-stimulating Peptide. *Nature* **1956**, *178* (4524), 90-90.
23. Sanger, F., The free amino groups of insulin. *Biochem J* **1945**, *39* (5), 507-515.
24. Allouche, A.-R., Gabedit—A graphical user interface for computational chemistry softwares. *Journal of Computational Chemistry* **2011**, *32* (1), 174-182.
25. Keeler, J., *Understanding NMR Spectroscopy* Wiley: 2002. (accessed 2021).
26. Jiang, H.; Kloc, C., Single-crystal growth of organic semiconductors. *MRS Bulletin* **2013**, *38* (1), 28-33.
27. Stock, N. L., Introducing Graduate Students to High-Resolution Mass Spectrometry (HRMS) Using a Hands-On Approach. *Journal of Chemical Education* **2017**, *94* (12), 1978-1982.
28. Elgrishi, N.; Rountree, K. J.; McCarthy, B. D.; Rountree, E. S.; Eisenhart, T. T.; Dempsey, J. L., A Practical Beginner's Guide to Cyclic Voltammetry. *Journal of Chemical Education* **2018**, *95* (2), 197-206.
29. Zittel, H. E.; Miller, F. J., A Glassy-Carbon Electrode for Voltammetry. *Analytical Chemistry* **1965**, *37* (2), 200-203.
30. Mendkovich, A. S.; Syroeshkin, M. A.; Mikhailchenko, L. V.; Mikhailov, M. N.; Rusakov, A. I.; Gul'tyai, V. P., Integrated Study of the Dinitrobenzene Electroreduction Mechanism by Electroanalytical and Computational Methods. *International Journal of Electrochemistry* **2011**, *2011*, 346043.
31. Fry, A. J.; Reed, R. G., Electrochemical reduction of imines in dimethylformamide. *Journal of the American Chemical Society* **1969**, *91* (23), 6448-6451.

Supporting Information

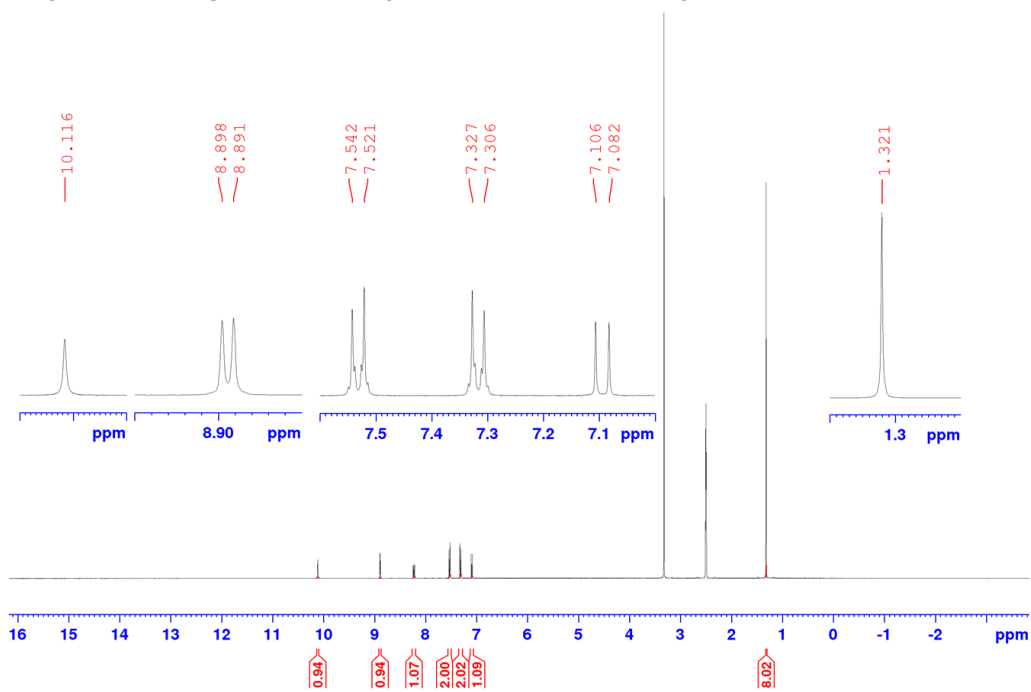


SI 1: COSY NMR (400 MHz, DMSO-d₆)
Spectrum of Model Compound



SI 2: HSQC NMR spectrum of
Model Compound

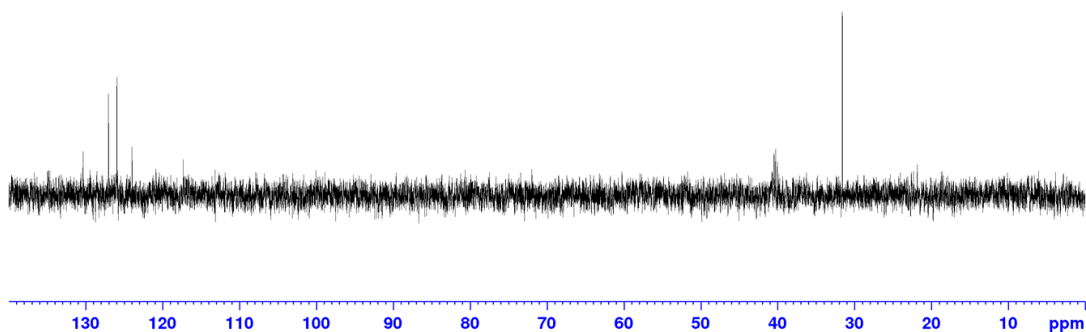
Orange PPT from t-butyl aniline and Sangers Rxn. Pure in DMSO Proton Spectra



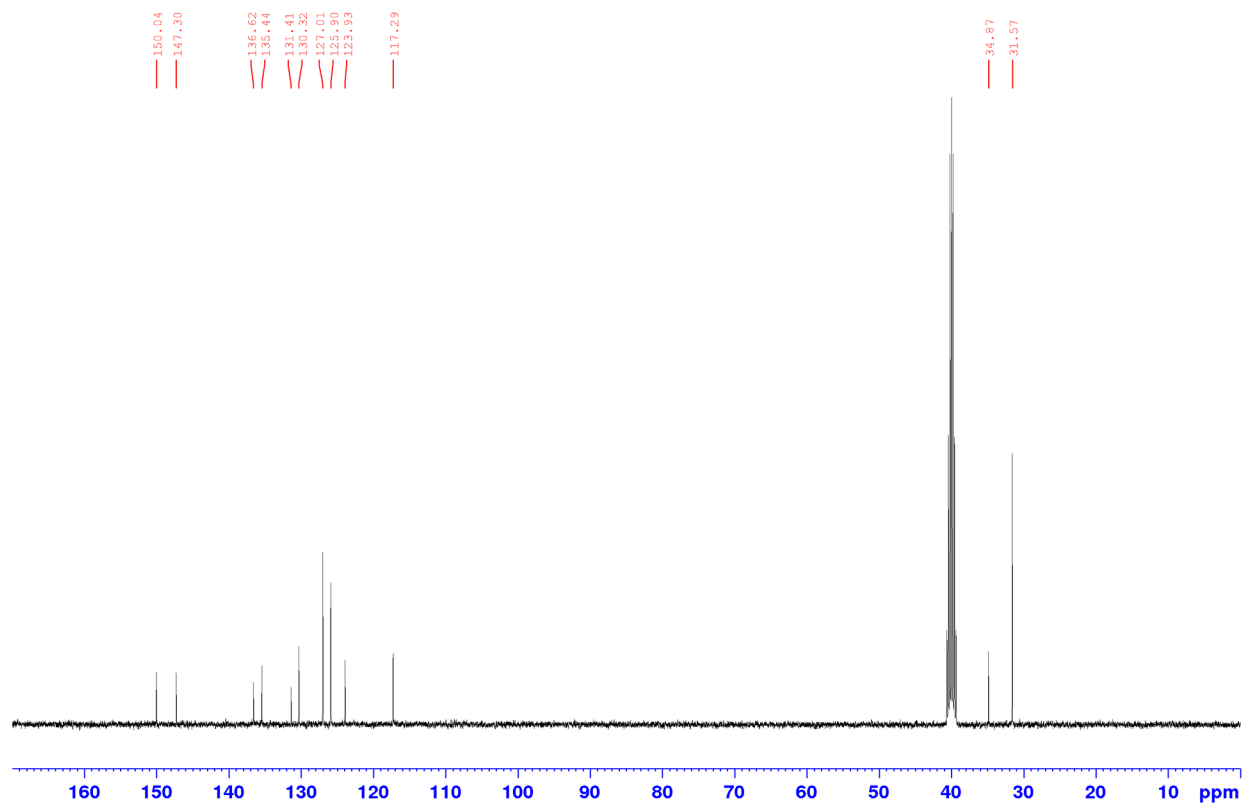
SI 3: ^1H NMR (400 MHz, DMSO-d_6) of Model Compound

Chemical shift values (ppm): 130.36, 127.00, 125.91, 123.94, 117.32.

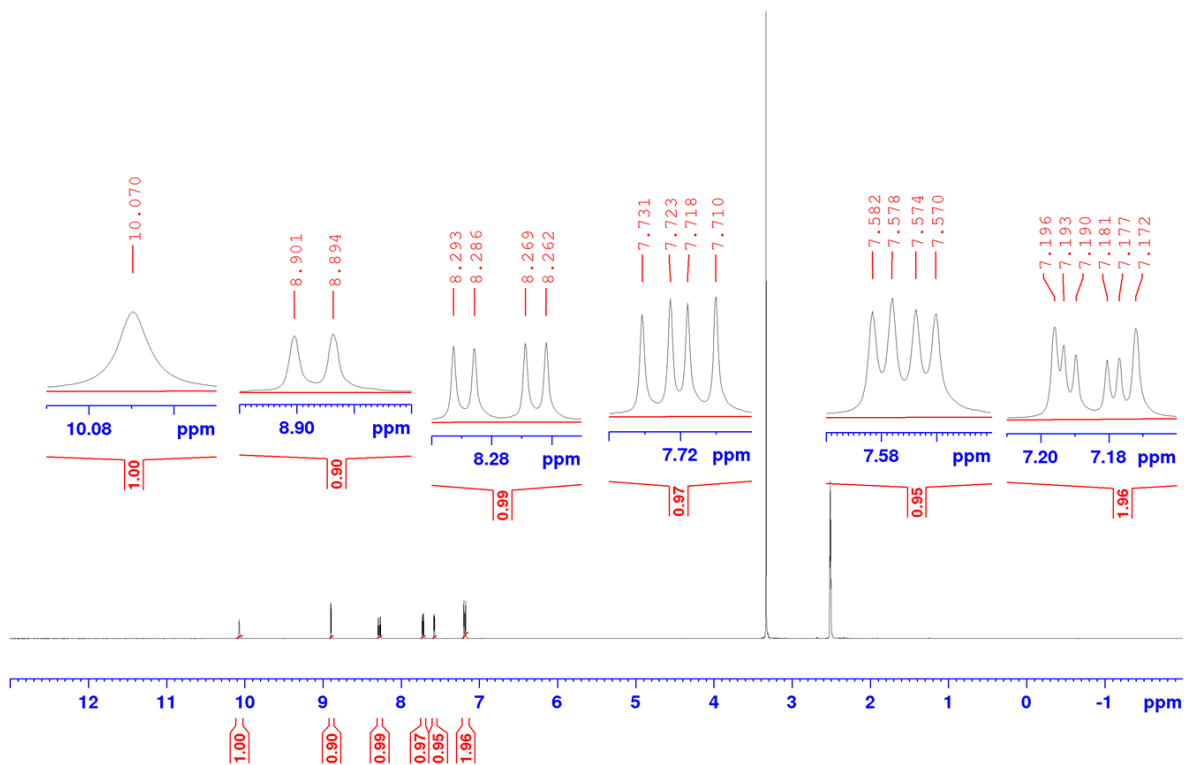
Chemical shift value (ppm): 31.63.



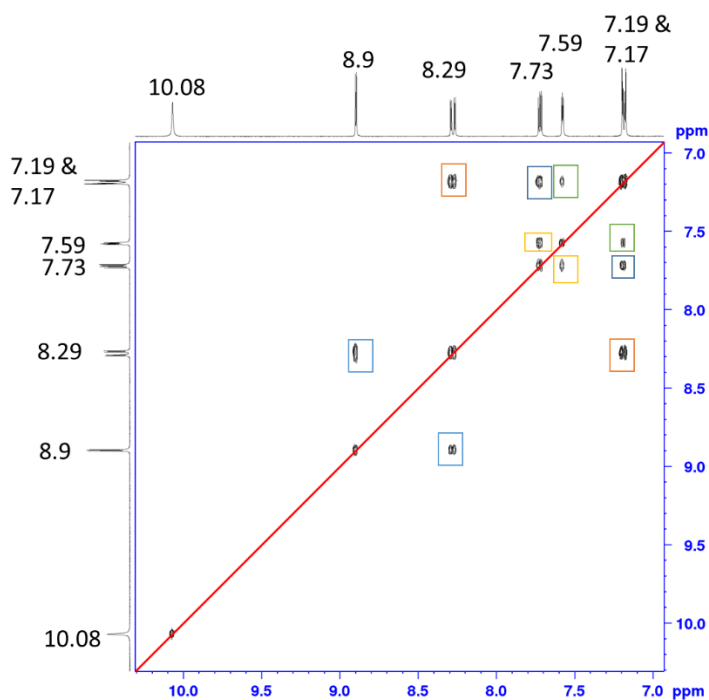
SI 4: ^{13}C DEPT 135 NMR (1400 MHz, DMSO-d_6) Spectrum of Model Compound



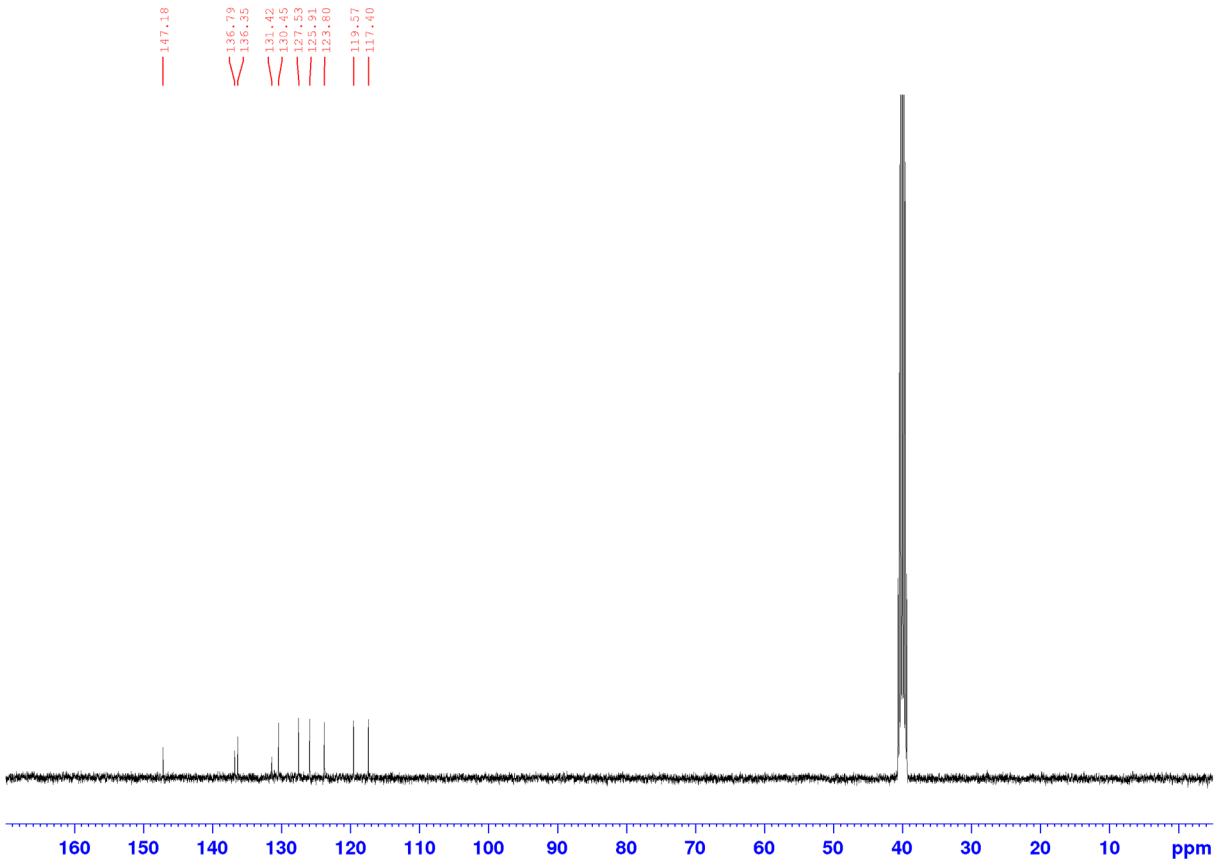
SI 5: ^{13}C Spectrum of Model Compound (1400 MHz – DMSO)



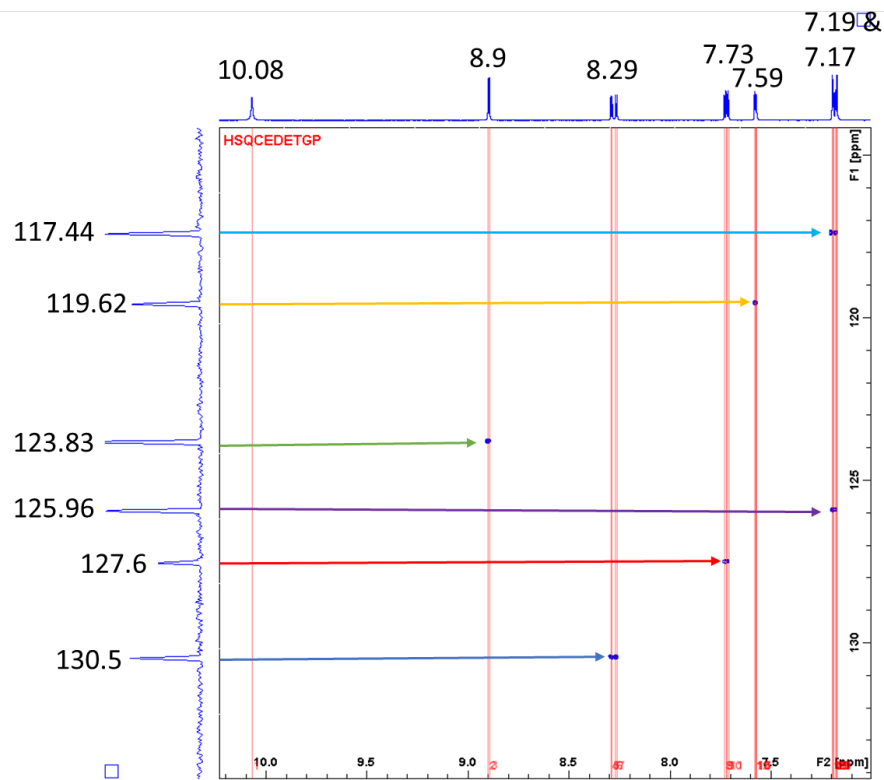
SI 6: ^1H NMR (400 MHz, DMSO-d_6) of Monomer 1



SI 7: COSY NMR (400 MHz, DMSO-d_6) Spectrum of Monomer 1

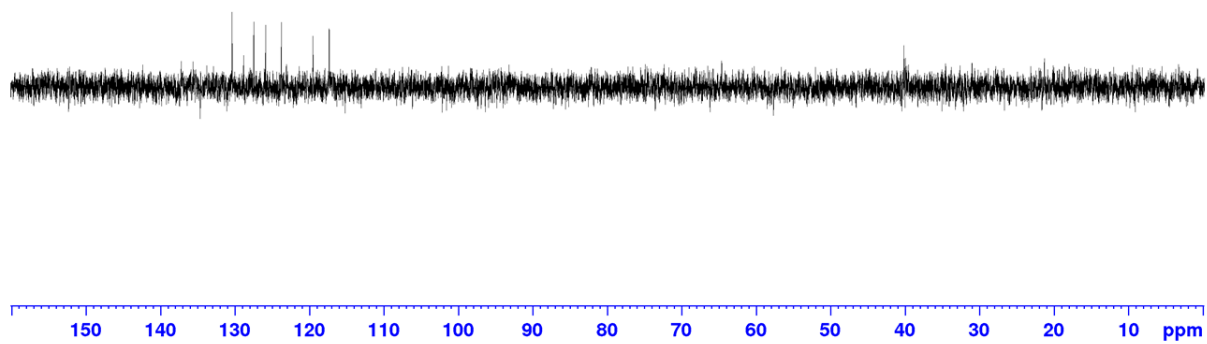


SI 8: ^{13}C Spectrum of Monomer 1 (1400 MHz -DMSO)



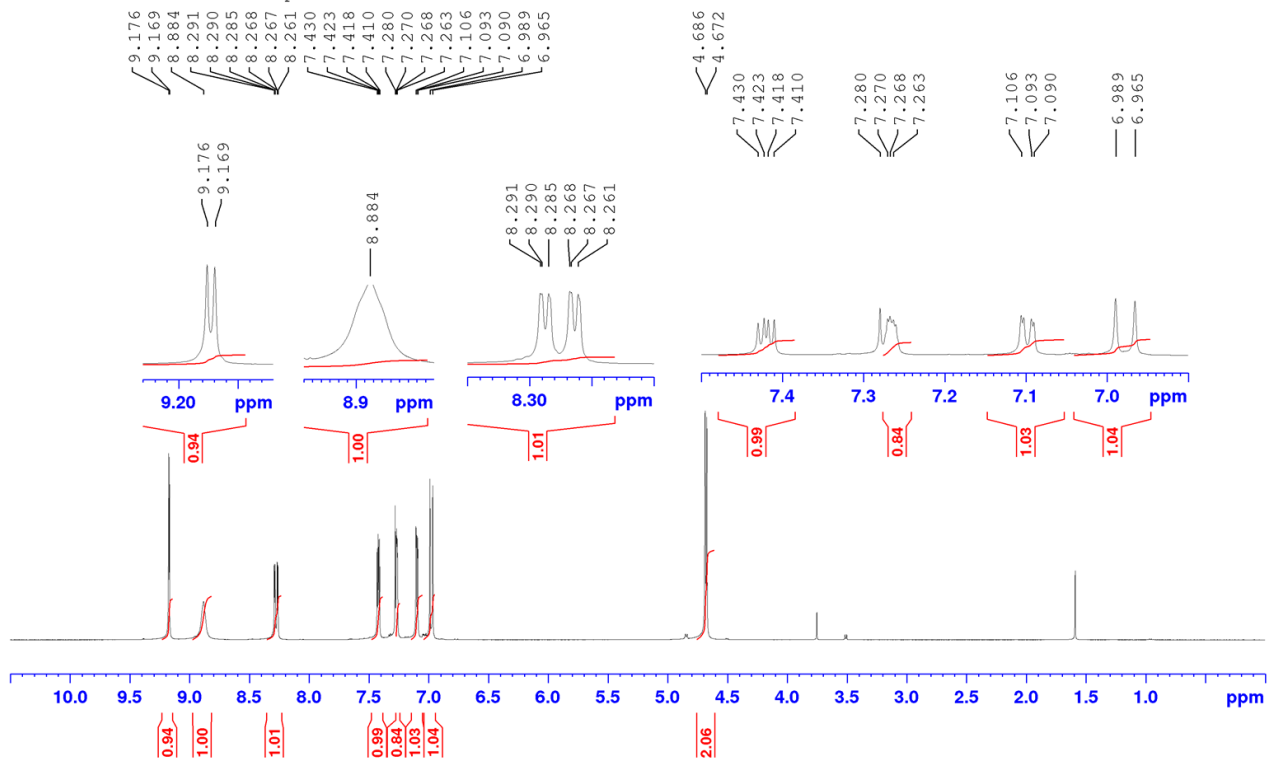
SI 9: HSQC NMR Spectrum of Monomer 1

130.46
127.54
125.93
123.82
119.60
117.41

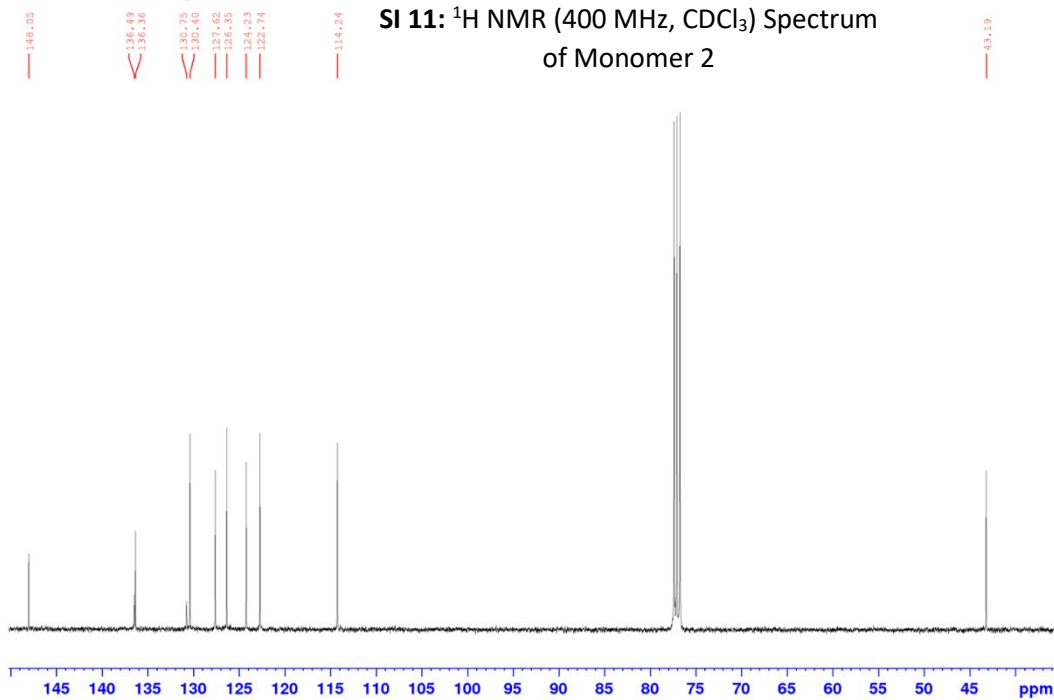


SI 10: ^{13}C DEPT NMR Spectrum of Monomer 1

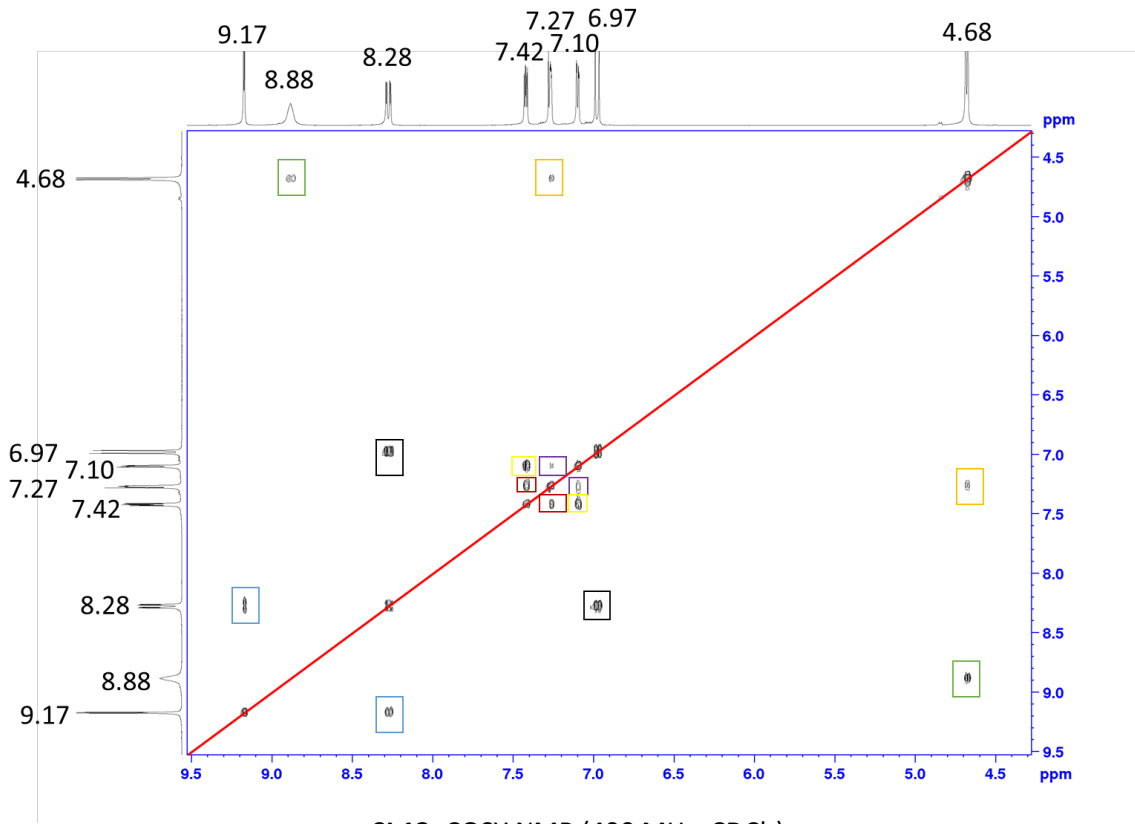
Yellow CDCl₃ Proton Spectra



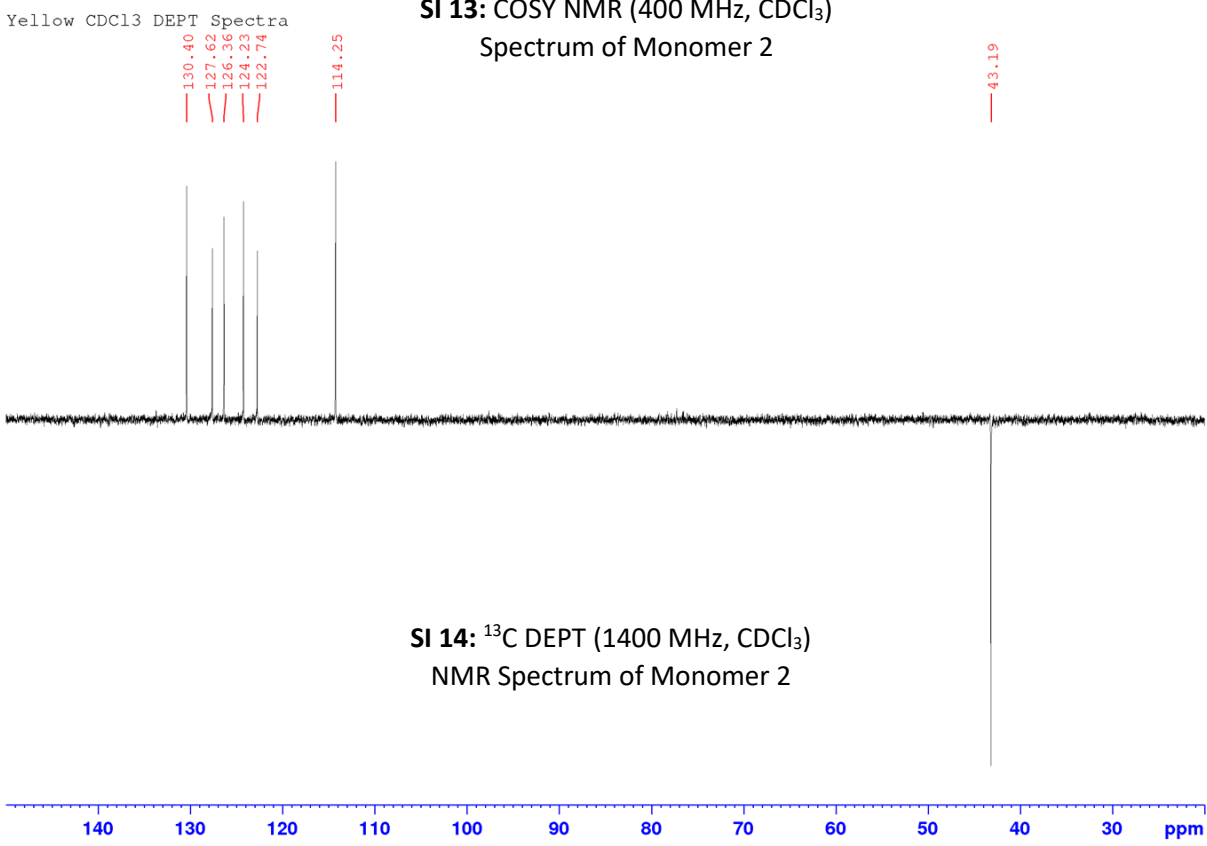
SI 11: ¹H NMR (400 MHz, CDCl₃) Spectrum of Monomer 2

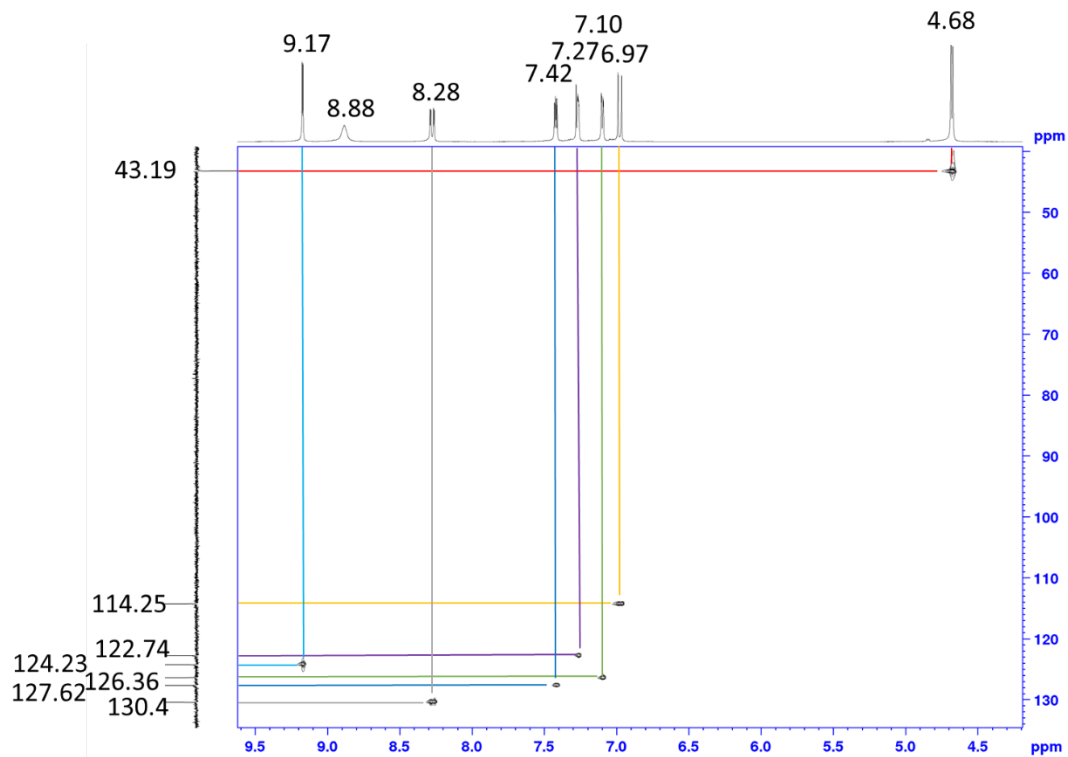


SI 12: ¹³C NMR (1400 MHz, CDCl₃) Spectrum of Monomer 2

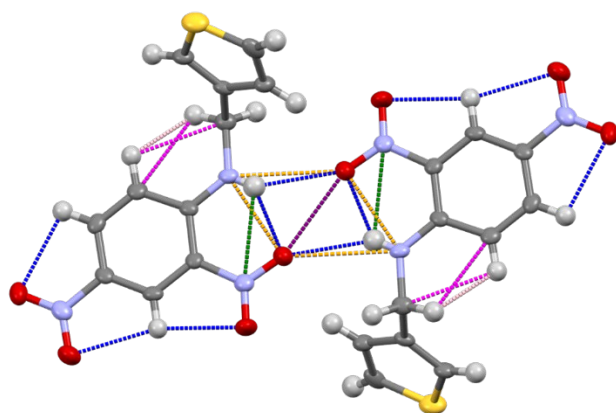


**SI 13: COSY NMR (400 MHz, CDCl₃)
Spectrum of Monomer 2**



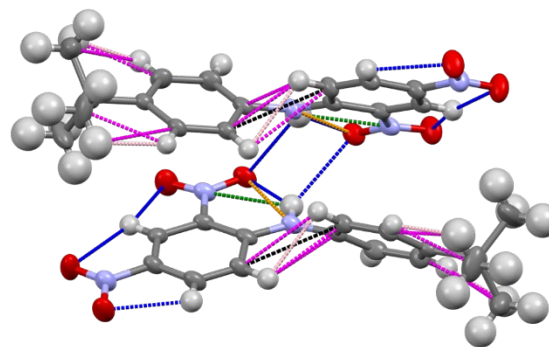


SI 15: HSQC NMR Spectrum of Monomer 2



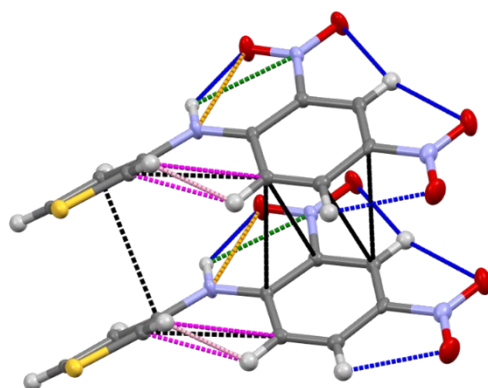
Blue: O---H short contacts
 Green: N---H short contacts
 Orange: N---O short contacts
 Purple: O---O short contact
 Magenta: C---H short contacts
 Pink: H---H short contacts

SI 16: Inter and intra-molecular interactions present in crystal structure of Monomer 2



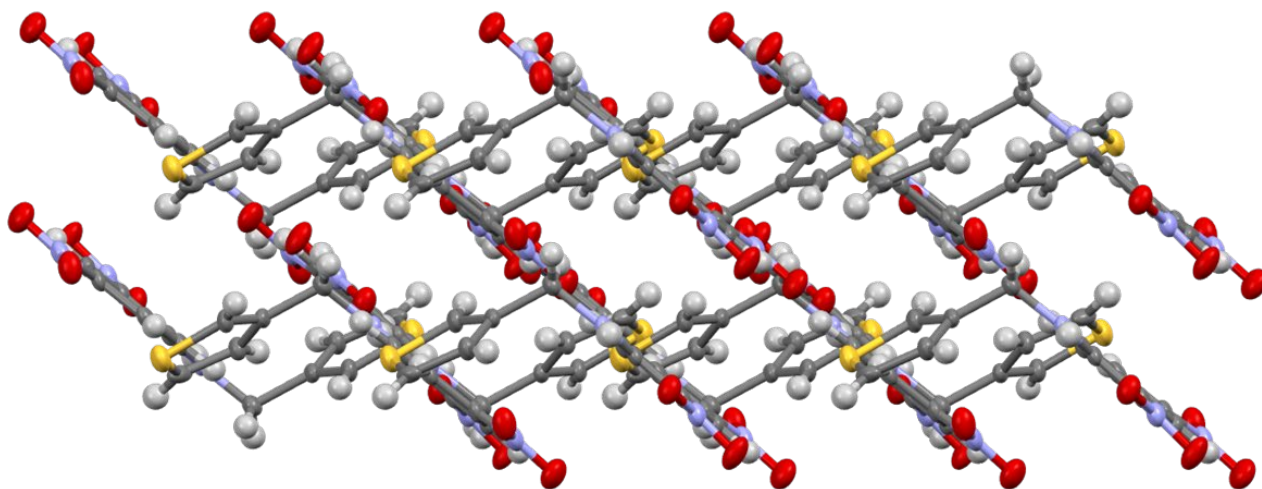
Blue: O---H short contacts
 Green: N---H short contacts
 Orange: N---O short contacts
 Purple: O---O short contact
 Magenta: C---H short contacts
 Pink: H---H short contacts
 Black: C---C short contacts

SI 17: Inter and intra-molecular interactions present in crystal structure of Model Compound

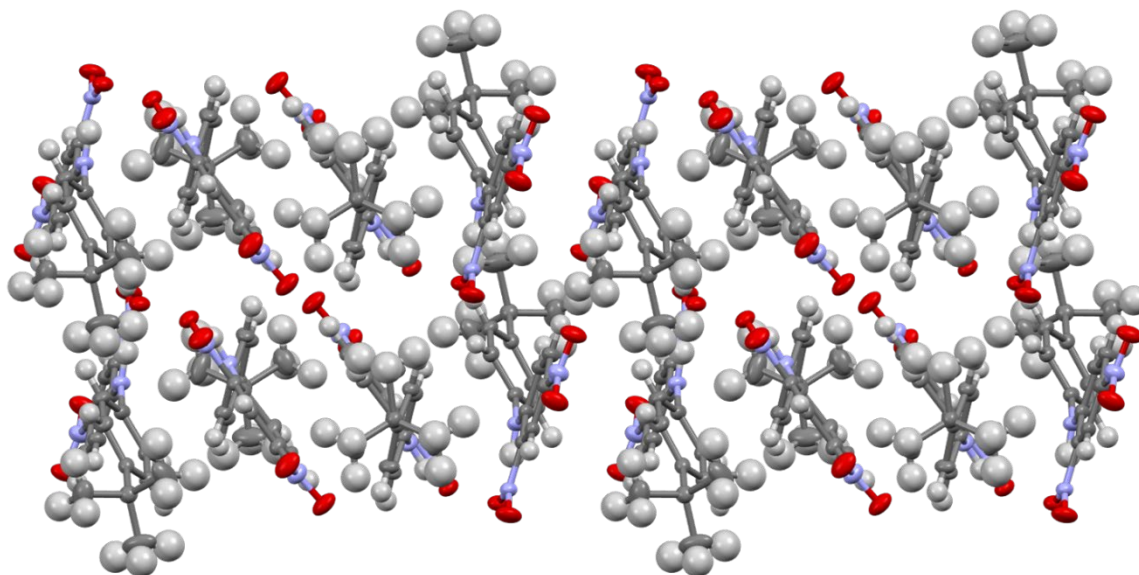


Blue: O---H short contacts
 Green: N---H short contacts
 Orange: N---O short contacts
 Magenta: C---H short contacts
 Pink: H---H short contacts
 Black: C---C short contacts

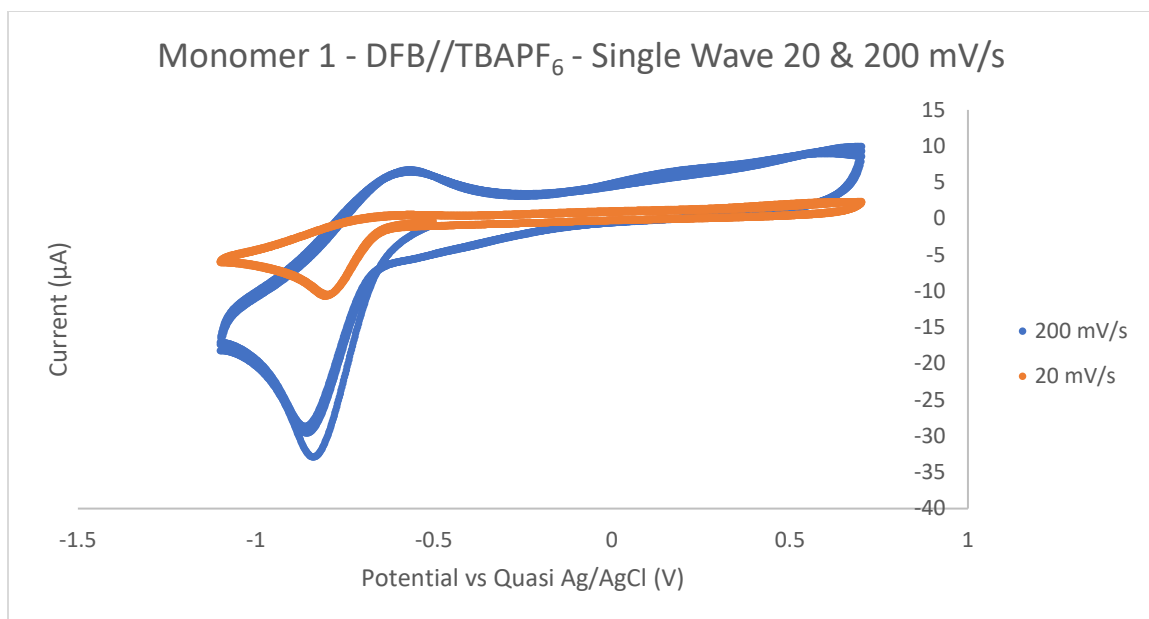
SI 18: Inter and intra-molecular interactions present in crystal structure of Monomer 1

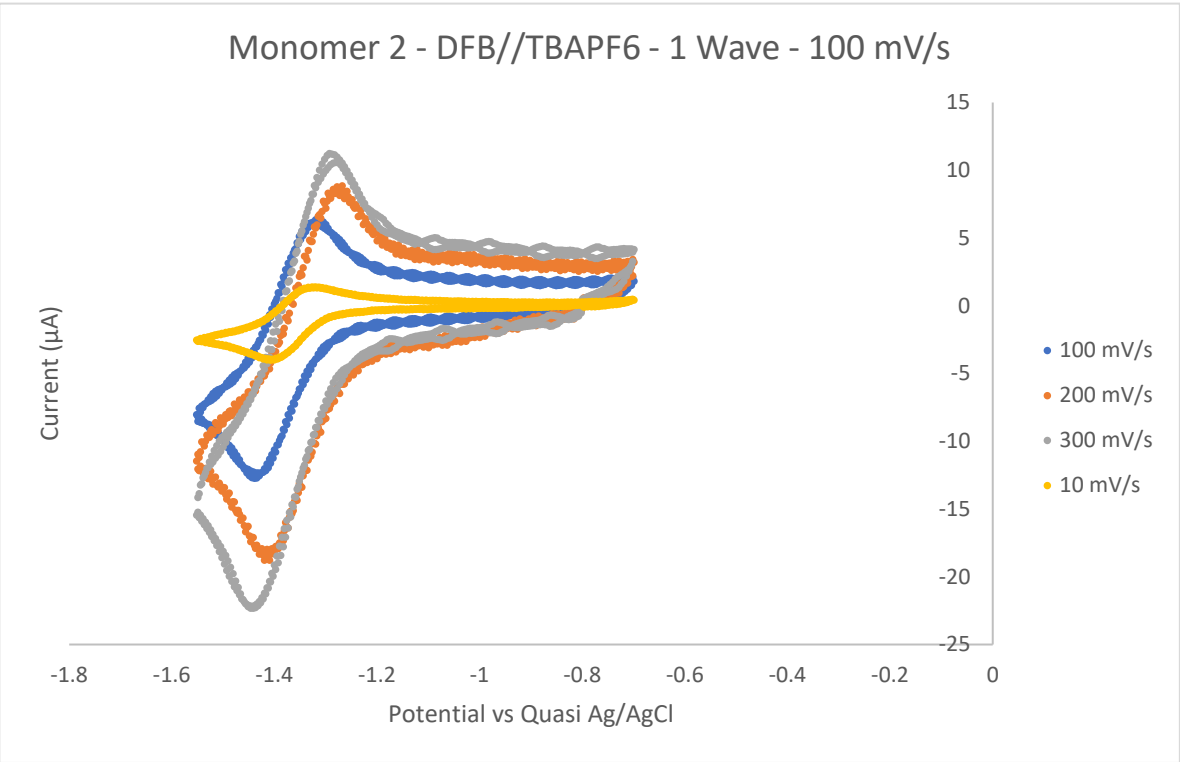
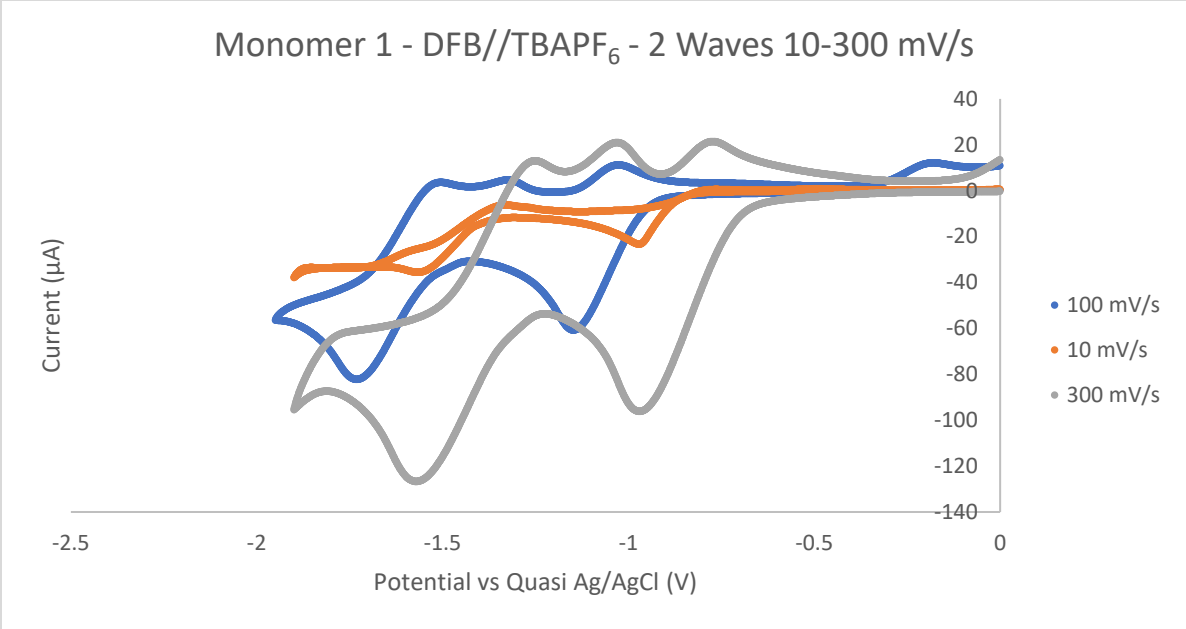


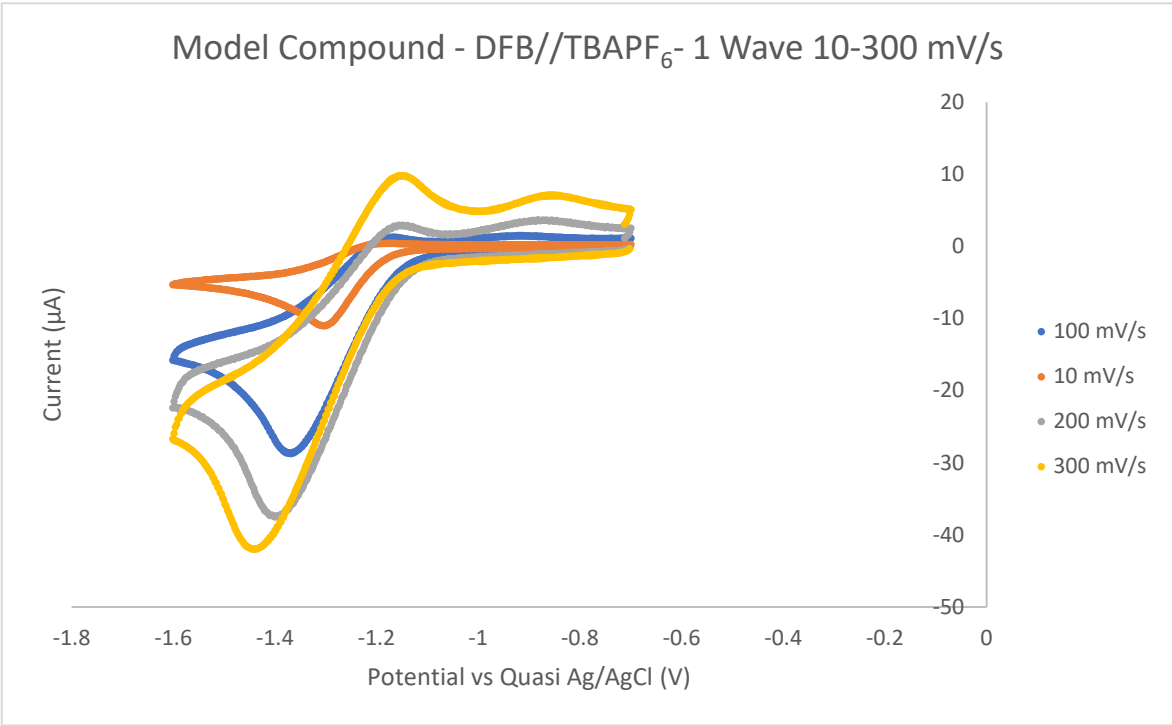
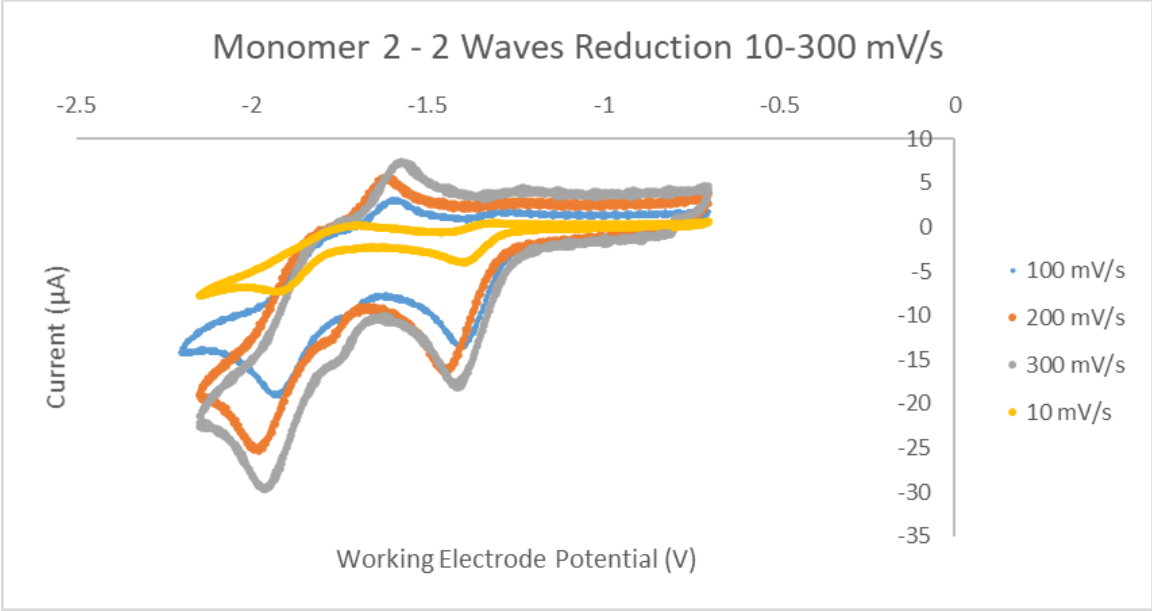
SI 18: Crystal packing of Monomer 2 along b axis.
Color Code: C-dark grey, H-light grey, N-purple, O-red,
S-yellow

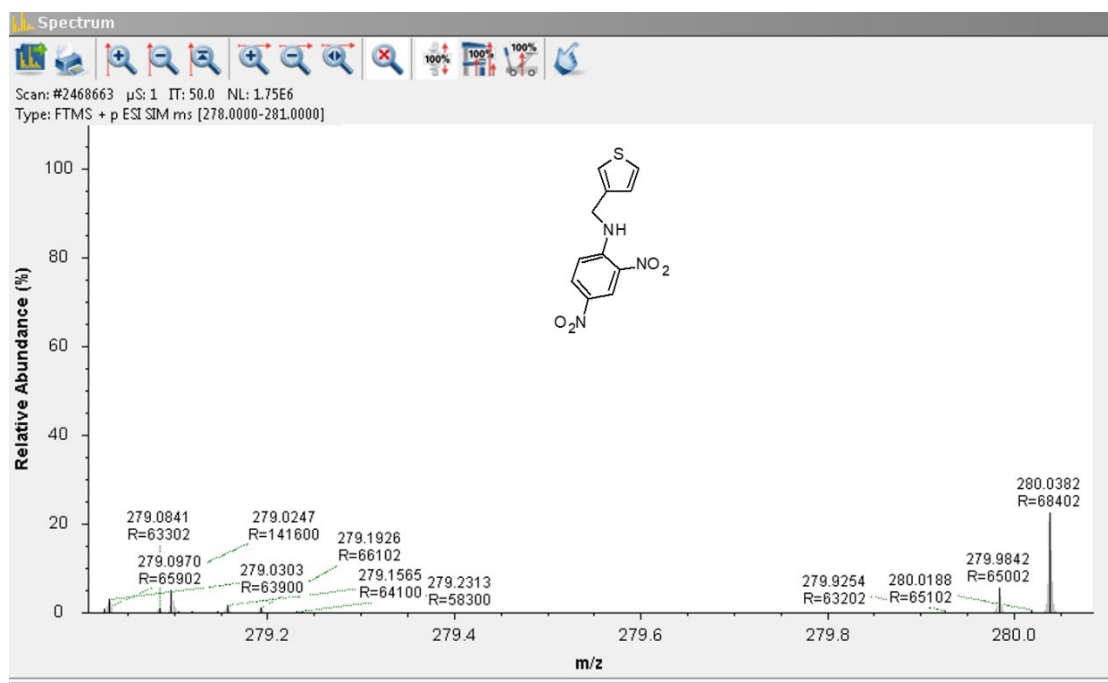
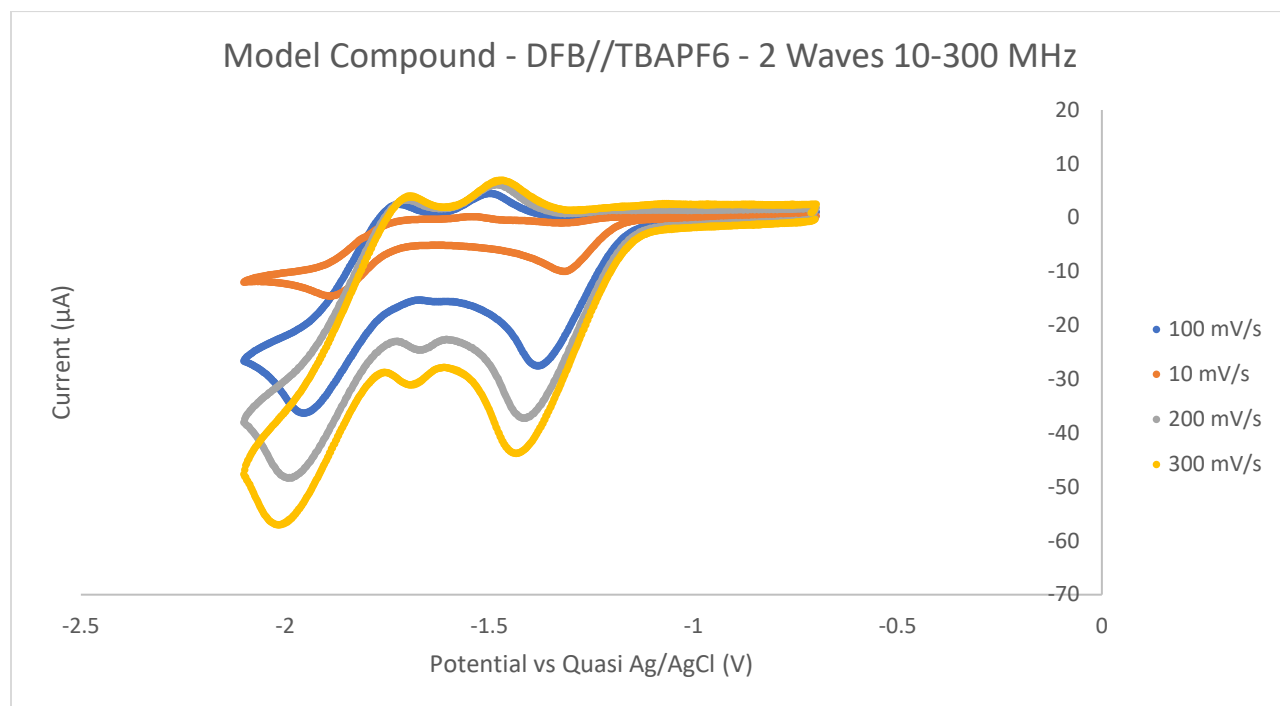


SI 19: Crystal packing of Model Compound along b-axis. Color Code: C-dark grey, H-light grey, N-purple, O-red









SI 20: HR-MS of Monomer 2